Sarah K. Carmichael, Johnny A. Waters, Cameron J. Batchelor, Drew M. Coleman, Thomas J. Suttner, Erika Kido, L.M. Moore, and Leona Chadimová, (2015) Climate instability and tipping points in the Late Devonian: Detection of the Hangenberg Event in an open oceanic island arc in the Central Asian Orogenic Belt, Gondwana Research

The copy of record is available from Elsevier (18 March 2015), ISSN 1342-937X, http://dx.doi.org/10.1016/j.gr.2015.02.009.

# Climate instability and tipping points in the Late Devonian: Detection of the Hangenberg Event in an open oceanic island arc in the Central Asian Orogenic Belt

Sarah K. Carmichael [a,*], Johnny A. Waters [a], Cameron J. Batchelor [a], Drew M. Coleman [b], Thomas J. Suttner [c], Erika Kido [c], L. McCain Moore [a], and Leona Chadimová [d]

[a] *Department of Geology, Appalachian State University, Boone, NC 28608, USA*
[b] *Department of Geological Sciences, University of North Carolina - Chapel Hill, Chapel Hill, NC 27599-3315, USA*
[c] *Karl-Franzens-University of Graz, Institute for Earth Sciences (Geology & Paleontology), Heinrichstrasse 26, A-8010 Graz, Austria*
[d] *Institute of Geology ASCR, v.v.i., Rozvojova 269, 165 00 Prague 6, Czech Republic*

* Corresponding author at: ASU Box 32067, Appalachian State University, Boone, NC 28608, USA. Tel.: +1 828 262 8471. E-mail address: carmichaelsk@appstate.edu (S.K. Carmichael).

***Article history:***
*Received 31 October 2014*
*Received in revised form 6 Feb 2015*
*Accepted 13 February 2015*
*Handling Editor: W.J. Xiao*

***Keywords:***
*Devonian–Carboniferous*
*Chemostratigraphy*
*Central Asian Orogenic Belt*
*West Junggar*
*Hangenberg Event*

## Graphical Abstract

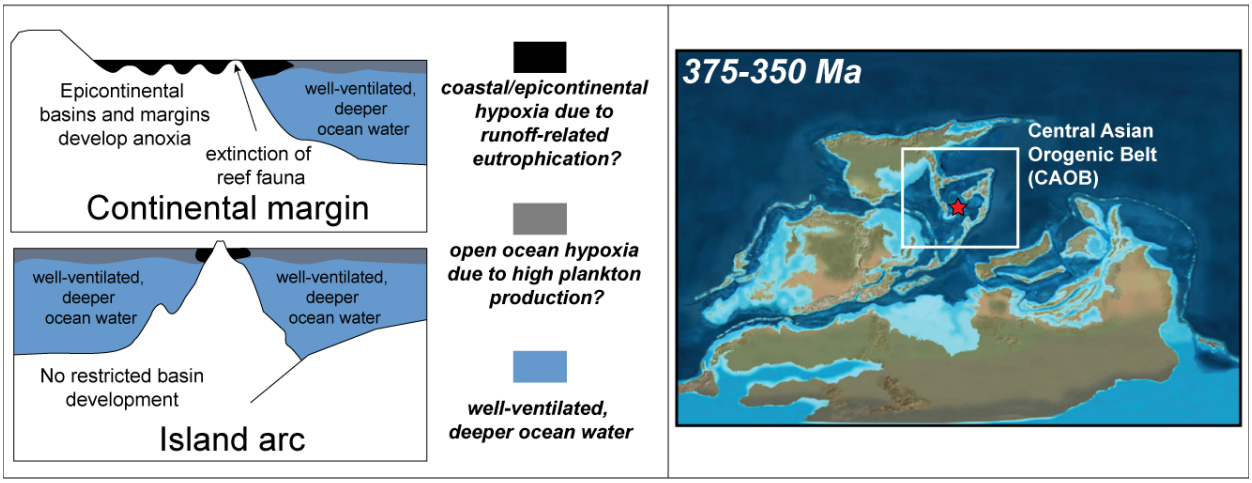


## Abstract

Sedimentary petrology and trace element geochemistry indicate that the Late Devonian to Early Carboniferous Heishantou Formation near Boulongour Reservoir (NW Xinjiang, China) was deposited on a steep slope, mid-latitude accreting island arc complex in an open oceanic system. Bulk $^{87}Sr/^{86}Sr$ ratios show excursion patterns that are consistent with excursions at the Devonian–Carboniferous (D–C) boundary in epicontinental margin sediments. Sedimentation rates for the Boulongour Reservoir sediments show highly variable rates that range from 0.5 cm/ky to 10 cm/ky, consistent with other Late Devonian sections and modern arc environments. Multiple whole rock geochemical proxies for anoxia and the size and distribution of pyrite framboids suggest the presence of the Hangenberg Event in the sediments associated with the D–C boundary, despite the lack of visible black shale. The presence of anoxia in an open ocean, island arc environment cannot be explained by upwelling of anoxic bottom waters at this paleolatitude, but can be explained by the global infliction of oceanic shallow water eutrophication on to a climate system in distress.

## 1. Introduction

The Late Devonian was a time of intense ecological crisis in both terrestrial and marine ecosystems. It is bracketed by two oceanic anoxia events that are associated with major mass extinctions. The Kellwasser Event at the Frasnian–Famennian (F–F) boundary decimated coral reef and other benthic marine communities (Copper, 1994) while slightly older extinctions decimated terrestrial ecosystems (Stigall, 2012 and McGhee, 2013). In contrast, the Hangenberg Event at the Devonian–Carboniferous (D–C) boundary primarily affected pelagic marine communities including fish (Sallan and Coates, 2010) and cephalopods (Becker, 1993 and Zong et al., 2014). In fact, a revised taxonomic severity ranking places the end Famennian (D–C boundary) and F–F extinction events as the fourth and fifth largest biodiversity crises in the Phanerozoic, respectively (McGhee et al., 2013, Table 3). These ocean anoxia events are also associated with a series of transgressions and regressions (Becker et al. (2012) and references therein), with the Hangenberg Event resulting from global cooling and the onset of glaciation at the end of the Famennian (Isaacson et al., 2008, Brezinski et al., 2009, Brezinski et al., 2010, Myrow et al., 2014 and Cole et al., 2015). The trigger for these anoxia events in the Late Devonian has long been debated (Racki, 2005), with proposed mechanisms ranging from the evolution of land plants (causing both a drawdown of atmospheric CO2 and the influx of nutrients into the oceans) (Algeo and Scheckler, 1998) to tectonic influence (Copper, 1986) to orbital forcing (De Vleeschouwer et al., 2013), to the influence of large igneous provinces (Bond and Wignall, 2014).

Regardless of trigger mechanism, many studies have concluded that upwelling of anoxic bottom waters was responsible for the widespread ocean anoxia in the Late Devonian (Caplan et al., 1996, McGhee, 1996, Caplan and Bustin, 1999, Cramer et al., 2008 and Formolo et al., 2014), while others have invoked sea level rise and resulting water column stagnation within epicontinental basins as a causal mechanism (Bond et al., 2004 and Bond and Wignall, 2008). Until recently, all of the studies of the Late Devonian anoxia events have been conducted on continental margins or in epicontinental basins, primarily in North America (Geldsetzer et al., 1993, Caplan et al., 1996, Caplan and Bustin, 1998, Smith and Bustin, 1998, Murphy et al., 2000, Caplan and Bustin, 2001, Rimmer, 2004, Rimmer et al., 2004, Bond and Wignall, 2005, Algeo et al., 2007, Algeo and Maynard, 2008, Cramer et al., 2008, Perkins et al., 2008, Schieber, 2009, Myrow et al., 2011, Bond et al., 2013, Tuite and Macko, 2013, Myrow et al., 2014, Cole et al., 2015 and Whalen et al., 2015) and Europe (Joachimski and Buggisch, 1993, Schindler, 1993, Racki et al., 2002, Bond et al., 2004, Brand et al., 2004, Gharaie et al., 2004, Kaiser et al., 2006, Pujol et al., 2006, Riquier et al., 2006, Marynowski and Filipiak, 2007, Azmy et al., 2009, Myrow et al., 2011, Kazmierczak et al., 2012, Chen et al., 2013, Kumpan et al., 2014a, Kumpan et al., 2014b and Matyja et al., 2015). Many of these study sites have been strongly influenced by increased sedimentation from the rising Appalachian Mountains. Additional studies have been conducted in locations that would presumably not be affected by the Appalachian/Variscan Orogenic Events, but all are associated with sediments derived from the cratonic blocks of Indochina (Hara et al., 2010 and Königshof et al., 2012), South China (Zheng et al., 1993, Chen et al., 2005, Gharaie et al., 2007, Du et al., 2008, Chen et al., 2013, Komatsu et al., 2014 and Whalen et al., 2015), Australia (Stephens and Sumner, 2003 and George et al., 2014), Russia/Siberia (Gutak et al., 2008, Izokh et al., 2009 and Tagarieva, 2013) and northern Africa (Kaiser et al., 2011). In contrast, only one study has unequivocally shown the presence of a Late Devonian anoxia event in an open oceanic setting far from continental-derived sediments: Carmichael et al. (2014) have documented the Kellwasser Event using multiple geochemical proxies within the Central Asian Orogenic Belt (CAOB), which therefore required an overhaul of the established models for ocean anoxia. To explain anoxia in the open ocean, Carmichael et al. (2014) suggested that the Kellwasser Event had to be caused by surface eutrophication rather than upwelling or basinal stagnation during transgressions. Earlier studies by Kido et al. (2013) and Suttner et al. (2014) have also suggested the presence of either the Hangenberg or Kellwasser Events in the CAOB based on field data and/or carbon and oxygen isotope data.

Although the Kellwasser Event is generally characterized by two organic rich black shale units, there is considerable variability in the expression of Hangenberg Event sediments, and this variability complicates not only its recognition in some sections, but in turn obscures the root cause (or causes) of this major ocean anoxia event. Many studies have specifically used the presence of a black shale facies to identify the Hangenberg Event and from there infer the presence of the D–C boundary (Caplan and Bustin, 1999, Rimmer, 2004, Perkins et al., 2008, Kaiser et al., 2011, Formolo et al., 2014, Komatsu et al., 2014, Kumpan et al., 2014a, Kumpan et al., 2014b and Myrow et al., 2014). However, some locations that span the D–C boundary do not contain black shale (Azmy et al., 2009, Kaiser et al., 2011, Myrow et al., 2011, Königshof et al., 2012, Kumpan et al., 2014a, Matyja et al., 2015 and Cole et al., 2015) due to their depositional environment. In the absence of a straightforward, visible manifestation of the Hangenberg Event in the form of a black shale bed or unconformity, the D–C boundary has historically been determined via conodont biostratigraphy (Flajs and Feist, 1988). However, the reliability of conodonts at the GSSP (La Serre section, Montagne Noire, France) has recently been demonstrated to be deeply problematic (Kaiser, 2009, Corradini et al., 2011 and Kaiser and Corradini, 2011). Becker et al. (2012) noted that the GSSP for the D–C boundary in the Montagne Noir must be reevaluated and Aretz (2013) has advocated the use of other fossils to define the D–C boundary. In the absence of appropriate fossil assemblages and visible black shales or unconformities, an alternative to biostratigraphy may be required in some sections to constrain both the Hangenberg Event and the D–C boundary.

Whole rock geochemistry and/or isotope chemostratigraphy have long been used in combination with biostratigraphy in many Late Devonian sections to develop global correlations across mass extinction intervals. Although positive $\delta^{13}C$ excursions in carbonate sediments have often been used to

denote the Hangenberg Event interval (Brand, 2004, Kaiser et al., 2006, Cramer et al., 2008, Kaiser et al., 2008, Königshof et al., 2012, Day et al., 2013, Kumpan et al., 2014b and Whalen et al., 2015), these excursions are variable depending on the carbonate material used (Buggisch and Joachimski, 2006), and may be obscured by diagenetic processes during local lowstands and therefore may not represent global marine signatures (Myrow et al., 2013). As other locations that cross the D–C boundary do not show noticeable positive excursions (Caplan et al., 1996, Buggisch and Joachimski, 2006, Kaiser et al., 2006, Kaiser et al., 2008, Azmy et al., 2009, Kumpan et al., 2014a, Kumpan et al., 2014b and Matyja et al., 2015), the use of $\delta^{13}$Ccarb as a correlative chemostratigraphic tool is limited at best. This is compounded by the problem that paleogeographic locations in the open ocean may record different $\delta^{13}$C signatures than those from within epeiric seas (Brand et al., 2009). The use of $\delta^{13}$Corg excursions in total organic carbon (TOC) has been used successfully in several studies across the D–C boundary (Caplan et al., 1996, Joachimski et al., 2001 and Kaiser et al., 2006) but its use (so far) has generally been limited to sections with visible organic-rich units, and therefore its use as a correlative tool across sediments without visible organic-rich units is not yet widespread.

In addition to carbon isotope stratigraphy, trends in $^{87}Sr/^{86}Sr$ have been used for chemostratigraphy as oceanic strontium isotope ratios have varied over time (McArthur et al., 2012). Brachiopods are the preferred material for obtaining $^{87}Sr/^{86}Sr$ in the Devonian (Becker et al., 2012), although there are very few measurements during the Famennian that have been fit to the accepted LOWESS curve (McArthur et al., 2012), and there are no accepted $^{87}Sr/^{86}Sr$ values for the latest Famennian above the crepida conodont zone (Van Geldern et al., 2006). Despite the apparent lack of data in the LOWESS database for this interval, three $^{87}Sr/^{86}Sr$ isotope studies specifically span the D–C boundary (Kürschner et al., 1993, Brand et al., 2004 and Azmy et al., 2009). Of these three studies, two show sharp $^{87}Sr/^{86}Sr$ excursions in conodont apatite at the D–C boundary from European sections (Kürschner et al., 1993) and in brachiopod calcite from locations in Europe and basins within North America ( Brand et al., 2004). The remaining study (also located in Europe) does not exhibit an $^{87}Sr/^{86}Sr$ isotope excursion (Azmy et al., 2009), although this can be explained by the presence of an unconformity within the section as well as biostratigraphic uncertainty about the exact location of the D–C boundary. The presence of a significant $^{87}Sr/^{86}Sr$ excursion in both brachiopods and conodonts across two continents suggests that these excursions are not local phenomena, and can be used for chemostratigraphic correlations in future studies.

Magnetic susceptibility (MS) measurements have long been used as a correlative tool in sedimentology (Hansen et al., 2000, Hladil et al., 2006, Da Silva et al., 2009, Riquier et al., 2010, Whalen and Day, 2010 and Ellwood et al., 2011). It is an excellent method for detecting sea level oscillations due to astronomical forcing (Ellwood et al., 2011, De Vleeschouwer et al., 2012 and De Vleeschouwer et al., 2013), and new research shows that the regression associated with the Hangenberg Event is easily detectable via MS (Day et al., 2013, De Vleeschouwer et al., 2013 and Whalen et al., 2015), which is particularly useful in sections where there is an absence of a visible unconformity or black shale facies.

Whole rock geochemistry and the presence and distribution of pyrite framboids have been used by many to characterize changes in redox conditions in Late Devonian marine black shales (Beier and Hayes, 1989, Pujol et al., 2006, Algeo and Maynard, 2008 and Marynowski et al., 2012). Even in the absence of visible black, organic-rich lithologies, the Kellwasser Event has been detected via whole rock geochemistry and/or pyrite framboid distribution in a variety of locations (Bond et al., 2004, Bond and Wignall, 2005, Bond et al., 2013, Carmichael et al., 2014 and George et al., 2014).

Here we propose a combined methodology to detect an "invisible" Hangenberg Event and the D–C boundary that incorporates sedimentology and chemostratigraphy ($^{87}Sr/^{86}Sr$ isotopes, magnetic susceptibility, and whole rock geochemistry) in a fundamentally different tectonic and depositional setting from previous studies of the Hangenberg Event, in an open ocean island arc complex in the Central Asian Orogenic Belt (CAOB). The presence of the Hangenberg Event in an open ocean environment such as this would indicate that ocean anoxia was global in scope, and that the mechanisms of anoxia invoked for sediments along continental margins and within continental basins are impossible for anoxia development in isolated island arc settings. If the Hangenberg Event is detected here, it is necessary to develop an alternative mechanism for anoxia during the Late Devonian.

## 2. Regional geology of the CAOB in northwestern China

The CAOB (a), a complex amalgamation of intra-oceanic island arcs and continental fragments, was formed prior to the end of the latest Carboniferous (Windley et al., 2007). Late Devonian to Early Carboniferous sediments in the Junggar Basin in Xinjiang Province, China (Fig. 1b) are exposed at the Boulongour Reservoir; these include the Zhulumute, Hongguleleng, Hebukehe, and Heishantou Formations (Ma et al., 2011, Suttner et al., 2014 and Zong et al., 2014). Tectonic models for the Late Devonian suggest that these sediments formed as part of the West Junggar/Balkash accretionary wedge (Fig. 2), deposited on a Marianas Island type island arc complex (Xiao et al., 2010, Choulet et al., 2012, Yang et al., 2013 and Xiao and Santosh, 2014). Preliminary geochemical work within the base of the Hongguleleng and Zhulumute Formations support a juvenile sediment source (such as arc volcanism) rather than cratonic erosion for these basal units (Carmichael et al., 2014), which is consistent with the tectonic interpretations of the region.

Typically, $\delta^{13}$C excursions are used in conjunction with other proxies to detect oceanic anoxia events, but the four $\delta^{13}$C analyses from the few limestones present in the Heishantou Formation did not exhibit any positive excursions in the expected Hangenberg Event interval (Suttner et al., 2014).

The inconclusive $\delta^{13}C$ measurements from this initial study are likely a sampling artifact due to the lack of limestone beds rather than evidence against the presence of the Hangenberg Event. To address this, our research group returned to the site in 2011 and re-measured a bed-by-bed stratigraphic section of the Heishantou Formation at the Boulongour Reservoir section (Fig. 3), which represents the continuity of the sedimentary sequence described in detail in Suttner et al. (2014).

Despite the lack of visible black shale units, the sediments exposed in the Boulongour Reservoir section do show evidence for other anoxia events through analysis of multiple geochemical and mineralogical proxies or through biostratigraphy. The Upper Kellwasser Event has been detected geochemically in the Hongguleleng Formation (Carmichael et al., 2014), and ammonoid biostratigraphy provides evidence for the Annulata Event in the Hebukehe Formation ( Zong et al., 2014).

### 3. Materials and methods

Samples were analyzed for major, trace, and rare earth elements, strontium isotopes, and mineralogy and mineral textures. Whole rock geochemical analyses were performed by Activation Laboratories (Ancaster, ON, Canada). Microtextures and mineral morphologies were imaged and analyzed via scanning electron microscopy with energy dispersive X-ray spectroscopy (SEM–EDS). SEM–EDS analyses were performed on a FEI Quanta 200

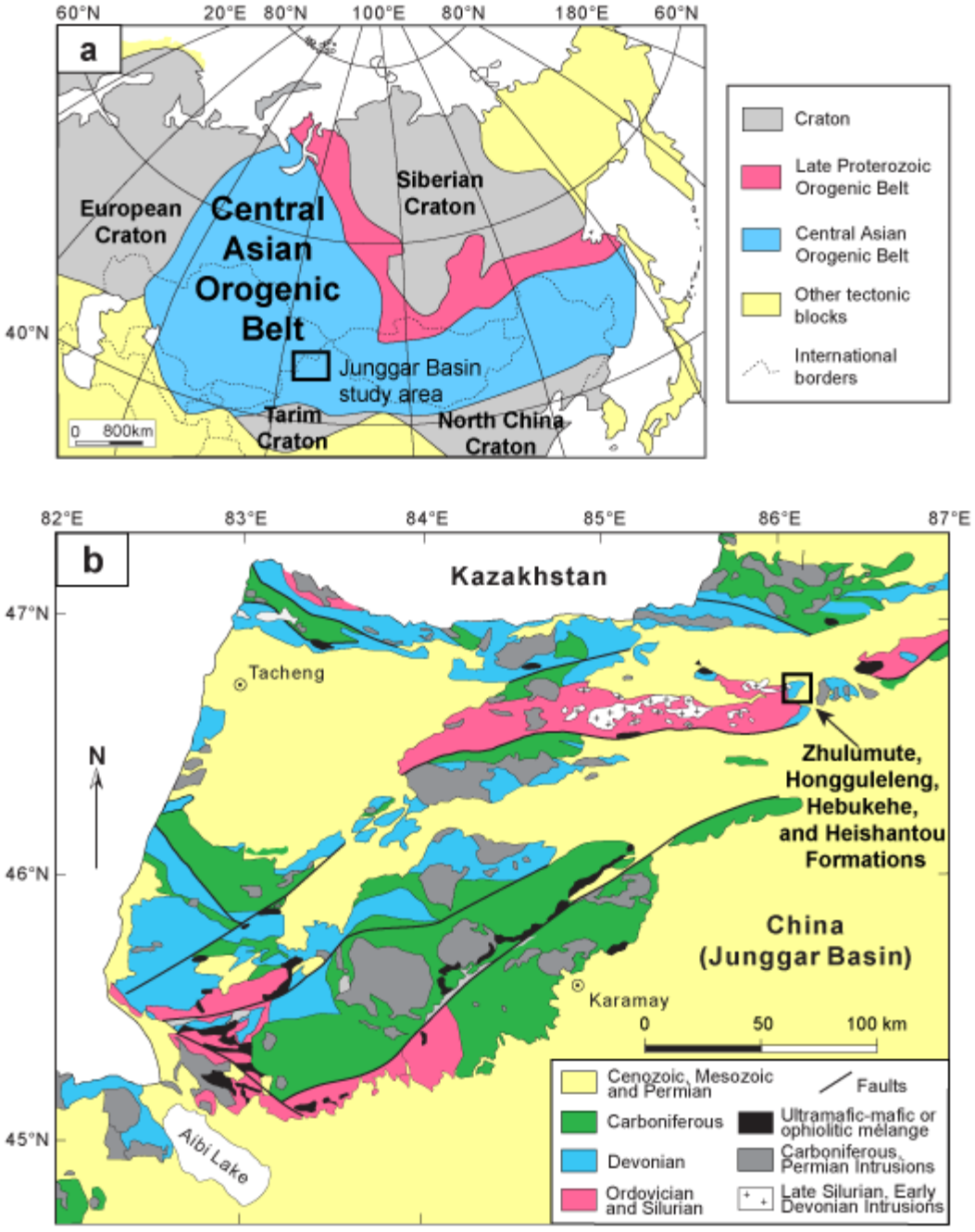


Fig. 1. a. Map of Central Asian Orogenic Belt (CAOB) showing the surrounding tectonic units (adapted from Yang et al. (2013)) and b. geologic map of the complex structural geology of the study area (modified from both Yang et al. (2013) and Choulet et al. (2012)).

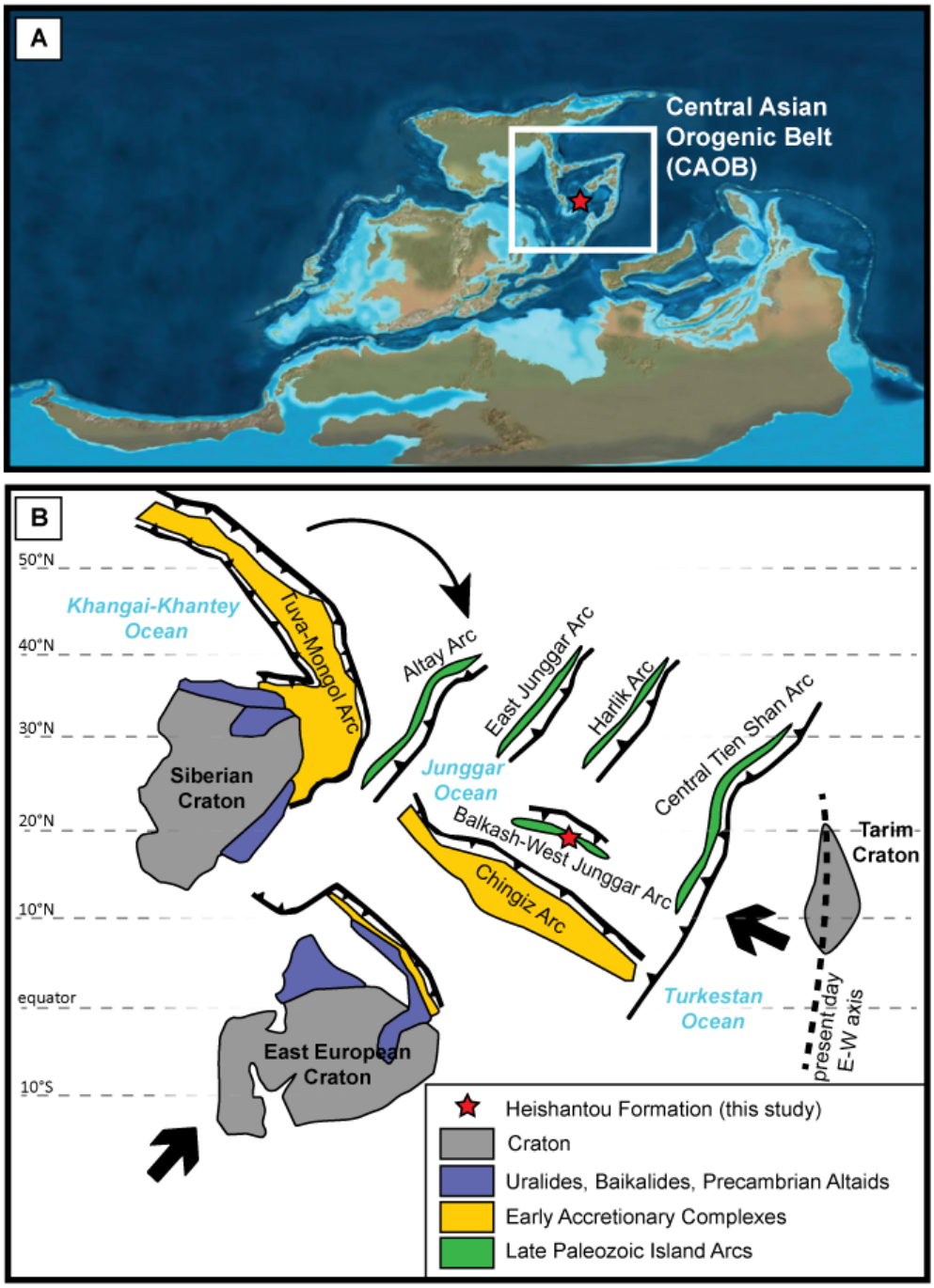


Fig. 2. Late Devonian paleogeographic model (A) and tectonic model (B) of the study area (shown by red star), indicating an amalgamating cluster of island arcs and accretionary complexes. Figure modified from Blakey (2008) and Xiao et al. (2010).

environmental scanning electron microscope with an attached EDAX energy-dispersive X-ray spectrometer and a Centaurus CL detector at Appalachian State University. Bulk mineralogy was measured with a Shimadzu XRD 6000 X-ray diffractometer and was confirmed using SEM–EDS analysis, also at the Appalachian State University.

All $^{87}Sr/^{86}Sr$ analyses were conducted at the University of North Carolina at Chapel Hill using a VG Sector 54 thermal ionization mass spectrometer (TIMS). Approximately 2–5 mg of powdered bulk rock sample was dissolved in 600 µL 3.5 N HNO3 for 24 h, and Sr was extracted from dissolved samples using EiChrom Sr-spec resin. In order to isolate carbonate Sr without leaching Sr from silicate minerals, 15 duplicate samples were analyzed using acetic acid instead of nitric acid; approximately 2–5 mg of powdered bulk rock sample was dissolved in 20 µL 3 N CH3COOH for 24 h at room temperature. The duplicate samples were centrifuged and the supernatant was extracted, dried and the residuum was redissolved in 3.5 M HNO3 in preparation for Sr extraction. The resultant solution was passed through a resin column filled with EiChrom Sr-spec resin. The resulting extraction was dried in 30 µL 2 M H3PO4, and the sample bead was loaded onto Re filaments using 2 µL each of TaCl5 and 2 M HCl. Samples were analyzed with an 88Sr ion intensity of 3 V (10− 11 Ω resistors) in triple dynamic mode.

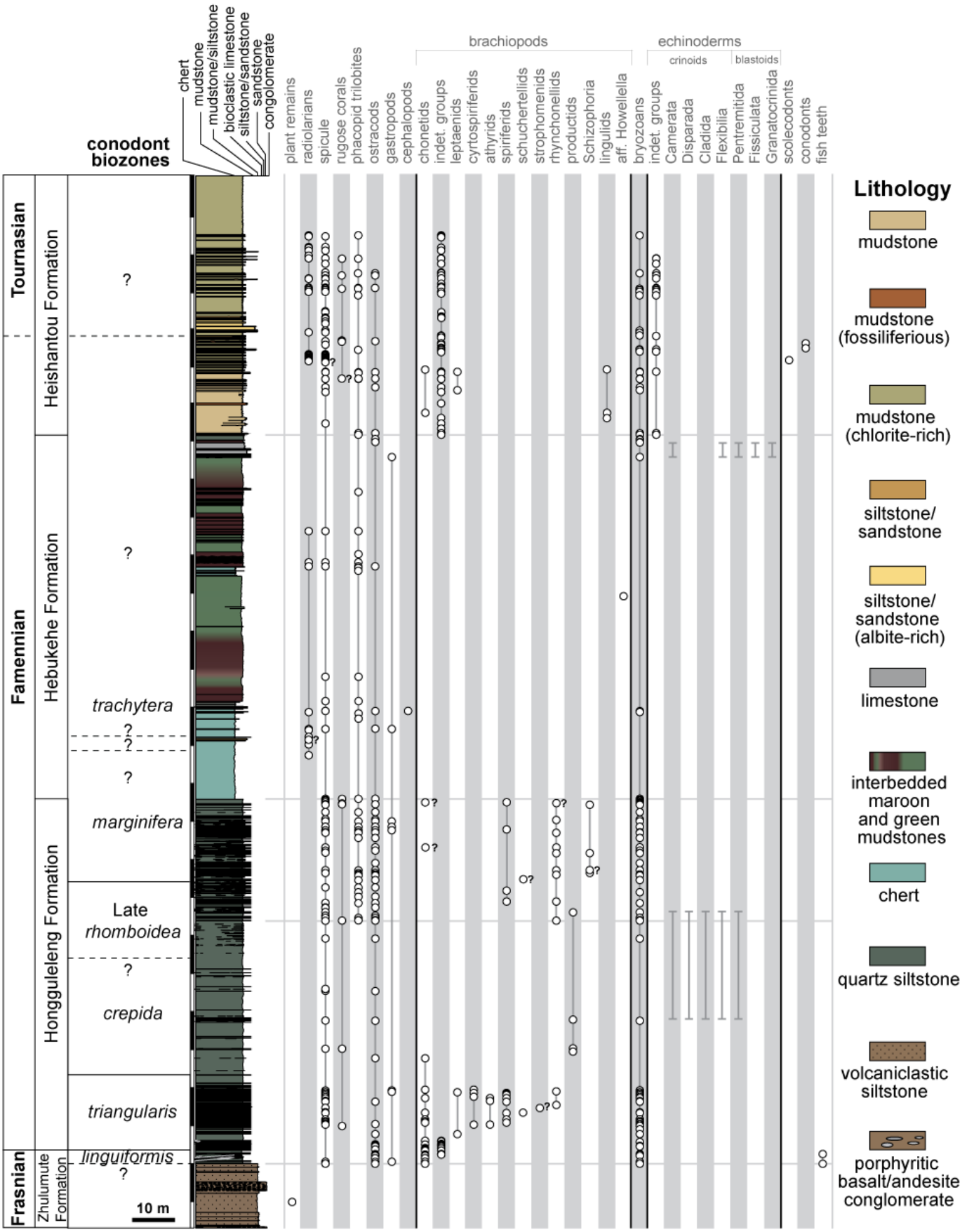


Fig. 3. Stratigraphic column of Boulongour Reservoir sediments and generalized faunal assemblages (modified from Suttner et al. (2014)). The Famenninan–Tournasian (D–C) boundary was tentatively identified in the field via brachiopod taxa (Ma et al., 2011).

To correct for mass fraction effects, Sr isotopic data were normalized to $^{86}Sr/^{88}Sr = 0.11940$. Measurements of NBS 987 on this instrument have a value of $^{87}Sr/^{86}Sr = 0.710258 \pm 0.000009$. The laboratory total procedure Sr blank fluctuates between 15 and 30 pg.

Rock specimens for MS analysis were cleaned of residues and weathered parts and formatted to 2 × 2 × 4 cm blocks at the University of Graz. MS of 119 rock specimens was measured using a MFK1-FA Kappabridge at Agico Inc. in Brno (Czech Republic) with a magnetic field intensity of 200 Am− 1 (peak value), operating frequency of 976 Hz, sensitivity of 2 × 10− 8 (SI), and accuracy within one range of ± 0.1%. Mass specific MS (MSchi) is expressed as 10− 9 m3kg− 1 for log plotting. MS is a physical quantity which expresses the magnetization acquired in material exposed to external magnetic field. The use of magnetization depends on the concentration, quality, grain size or morphology of magnetic component (magnetic particles in a form of minerals) in the studied sample.

For total organic carbon (TOC) and sulfur content, approximately 5 g of sample was crushed to a fine powder. Between 0.1 and 0.5 g of powder was treated 3 times with 2 N HCl for 24 h to remove carbonate material. The samples were then rinsed 3 times with distilled water to neutrality. The resulting dried powder was then analyzed with a LECO CS-300 combustion analyzer (version 1.0, Year 1992) at University of Graz. For each powdered sample this procedure was run three times to confirm powder homogeneity and to cross-check instrument reliability. The mean value for each sample based on these three runs is used in this study.

## 4. Results

### *4.1. Stratigraphy and sedimentology*

The stratigraphy of the Boulongour Reservoir sediments is discussed in Suttner et al. (2014); in this study we consider only the upper 53 m of a section that represents the Heishantou Formation (a marine sequence located below storm wave base) (Fig. 3). In the Heishantou Formation, there is no black shale bed to unequivocally denote the presence of the Hangenberg Event, and precise biostratigraphic control for the Devonian–Carboniferous boundary is lacking. The approximate location of the Hangenberg Event in the Boulongour Reservoir section has been very tentatively identified at approximately 26 m above the base of the Heishantou Formation (equivalent to 210 m above the base of the Hongguleleng Formation, at the Frasnian–Famennian boundary) using limited carbon isotope stratigraphy (Suttner et al., 2014) and brachiopod faunas (Ma et al., 2011), while ammonoid biostratigraphy in an associated Hebukehe section indicates that the Hangenberg Event may be located at the base of the Heishantou Formation (Zong et al., 2014).

The Heishantou Formation is composed primarily of mudstones and siltstones with several lenses of bioclastic mudstones and silty sandstones. Primary mineralogy includes albite, quartz, and chlorite with minor illite and trace apatite. Calcite is present in shell-rich beds within a muddy matrix. Albite is primarily exhibited as angular to sub-angular silt particles (< 100 μm diameter), while quartz is porous and microcrystalline (1–2 μm diameter) (Fig. 4). Some of clay-rich sediments show lamination, but most indicate that the presence of clay is due to in-situ weathering reactions of biotite or hornblende fragments or sequestered in mud pellets (up to 100 μm diameter) (Fig. 4). Microtextural analysis via scanning electron microscopy shows that some mudstones contain textures that suggest a turbidite origin, while other mudstones have a more uniform texture. Other samples indicate the presence of volcanic ash beds. Several particularly porous layers contain abundant titanite cements.

There is no field evidence for an unconformity within the Heishantou Formation (Suttner et al., 2014), but the distribution of calcite, albite, and chlorite changes at approximately 210 m, where the interbedded siltstones and bioclastic mudstones transition to mineralogically immature chlorite-rich siltstones with sandstone lenses and thin layers of volcanic ash and volcaniclastic silts (Fig. 5). This transition at 210 m from fine-grained bioclastic calcareous siltstones/wackestones (Suttner et al., 2014) to immature siltstones and sandstones (this study) is consistent with the changes in sedimentation seen at the D–C boundary or associated with the Hangenberg Event in other locations, where organic-rich mudrocks are overlain by sandstones (Caplan and Bustin, 1999, Kaiser et al., 2006, Kaiser et al., 2011 and Myrow et al., 2014), calcareous mudstones (Kaiser et al., 2008), and nodular siltstones (Algeo and Maynard, 2008). It is also consistent with the tentative location of the D–C boundary in the Heishantou Formation from biostratigraphy (Ma et al., 2011 and Zong et al., 2014).

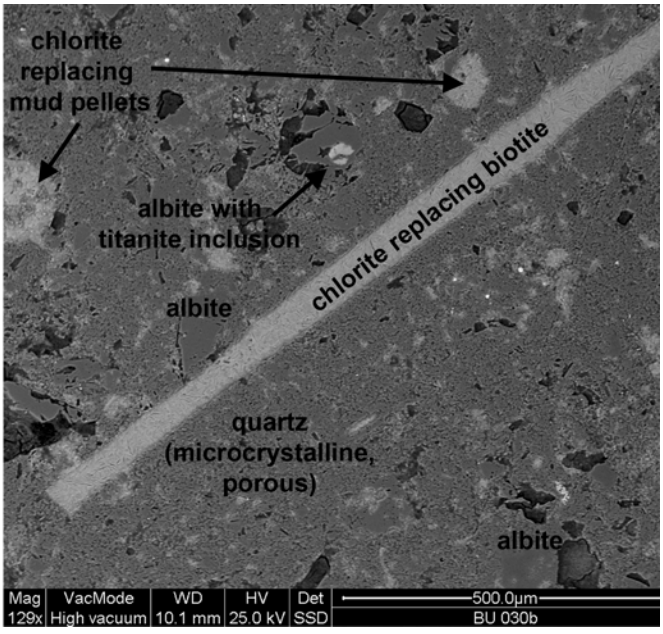


Fig. 4. Backscattered SEM–EDS image of typical mineral textures in the Heishantou Formation. Chlorite typically is found as pseudomorphs of mud pellets and detrital biotite flakes, or as rims on albite grains. Albite is found as angular to sub-angular silt sized particles (generally b100 μm diameter). Quartz is generally microcrystalline and somewhat porous. The immaturity of the sediment supports a nearby volcanic arc source.

### 4.2. Geochemical proxies for sediment source

Sediment source can be constrained with whole rock Th/U ratios (Carpentier et al., 2013), where a Th/U of ~ 3 in siliciclastic sediments indicates a juvenile sediment source such as a volcanic arc (Fig. 6). This result is consistent with previous work showing that the underlying Hongguleleng and Zhulumute Formations are derived from juvenile sediment sources as well (Carmichael et al., 2014). Additional trace element signatures within the detrital fraction of sediments, such as Hf/Th/Ta relationships (Wood, 1980) and La/Sc/Zr relationships (Bhatia and Crook, 1986) show an oceanic island and continental island arc sediment source for the Heishantou Formation sediments (Fig. 7a, b). The Ta/Yb and Nb/Y ratios (Pearce et al., 1984) likewise cluster within volcanic arc sources (Fig. 7c, d). These discrimination diagrams indicate that sediment sources derived from volcanic island arcs are present within the Heishantou Formation, an interpretation that is consistent with tectonic studies of the region that model arc evolution and microcontinental accretion in the CAOB at during the Late Devonian (Fig. 2) (Xiao et al., 2010, Choulet et al., 2012, Yang et al., 2013 and Xiao and Santosh, 2014).

### 4.3. $^{87}Sr/^{86}Sr$ isotope signatures

Nitric acid leaches of sediments show that $^{87}Sr/^{86}Sr$ ratios range from 0.70716 to 0.70928 within the sediments of the Heishantou Formation (Table 1), with a large positive excursion towards heavier $^{87}Sr$ values at approximately 212 m (within 2 m of the hypothesized location of the D–C boundary based on brachiopod, field, and textural observations) (Fig. 8). Acetic acid leaches target only the carbonate fraction of the sediment, and provide $^{87}Sr/^{86}Sr$ ratios of 0.70719–0.70815 (Table 2). Like the data from the nitric acid leaches, the acetic acid data also show a sharp excursion at 212 m. When compared against existing $^{87}Sr/^{86}Sr$ isotope oscillations and excursions in conodont apatite across the D–C boundary in Germany (Supplemental Information, Table S1; Kürschner et al., 1993) and from brachiopods from both the central United States and Europe (Supplemental Information, Table S2; Brand et al., 2004), both sets of $^{87}Sr/^{86}Sr$ values from the Heishantou Formation unequivocally support the location of the D–C at 212 m (Fig. 8). Furthermore, the $^{87}Sr/^{86}Sr$ ratios from the nitric acid leach from Heishantou Formation samples are remarkably similar to the $^{87}Sr/^{86}Sr$ isotopic signatures measured from conodont apatite (Fig. 8), although samples from the Heishantou Formation do show more extreme fluctuations. However, we are reluctant to use these new $^{87}Sr/^{86}Sr$ values as representative of oceanic water at the D–C boundary as the values are not consistent with the accepted LOWESS fit for $^{87}Sr/^{86}Sr$ in the Late Devonian (McArthur et al., 2001 and McArthur et al., 2012). As the Heishantou Formation is located in an active volcanic island arc system (Fig. 7), our lower $^{87}Sr/^{86}Sr$ signatures could represent localized phenomena due to submarine groundwater mixing with volcanogenically altered groundwater, similar to what is observed in modern day active margins (Kim et al., 2003). Furthermore, at the scale of our sample collection interval (particularly through the D–C boundary section) any submarine groundwater discharge or hydrothermal alteration would affect all samples similarly, preserving the oscillations but not the original oceanic $^{87}Sr/^{86}Sr$ ratios. We see neither field nor microscopic evidence for localized (cm-scale) faulting, excessive

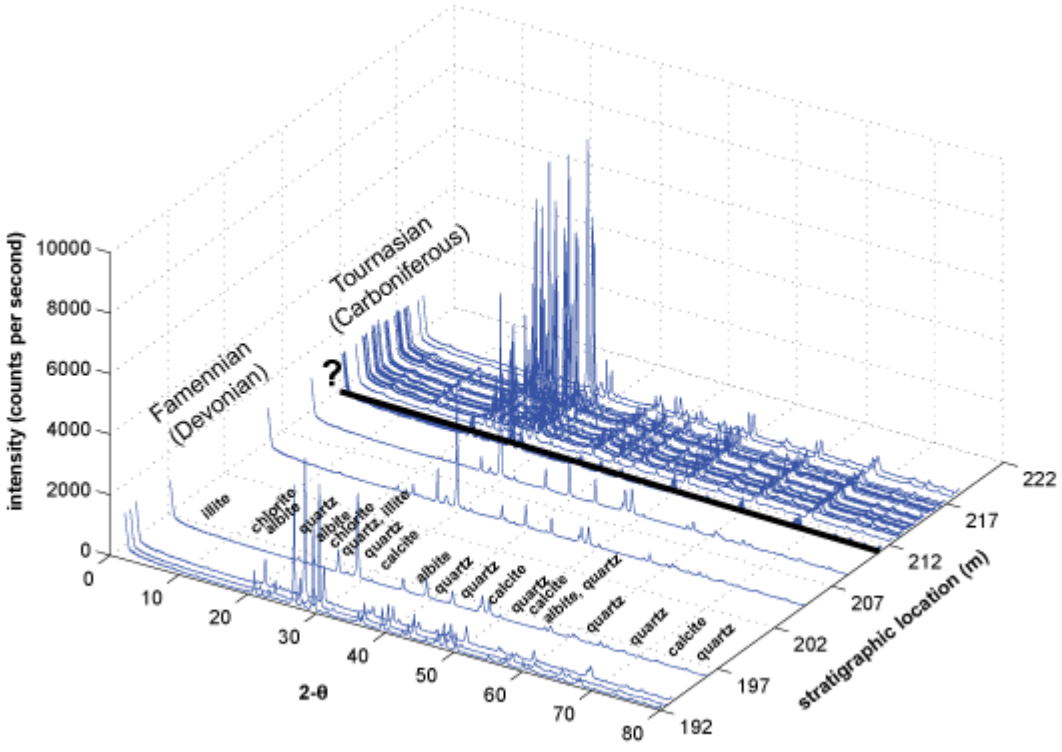


Fig. 5. X-ray diffraction (XRD) patterns of bulk sediments from the lower 30 m of the Heishantou Formation show no appreciable difference in mineralogy throughout the section, only a difference in the distribution of minerals (particularly calcite, chlorite, and albite). Mineralogy as identified using XRD data was confirmed using scanning electron microscopy with energy dispersive X-ray microanalysis

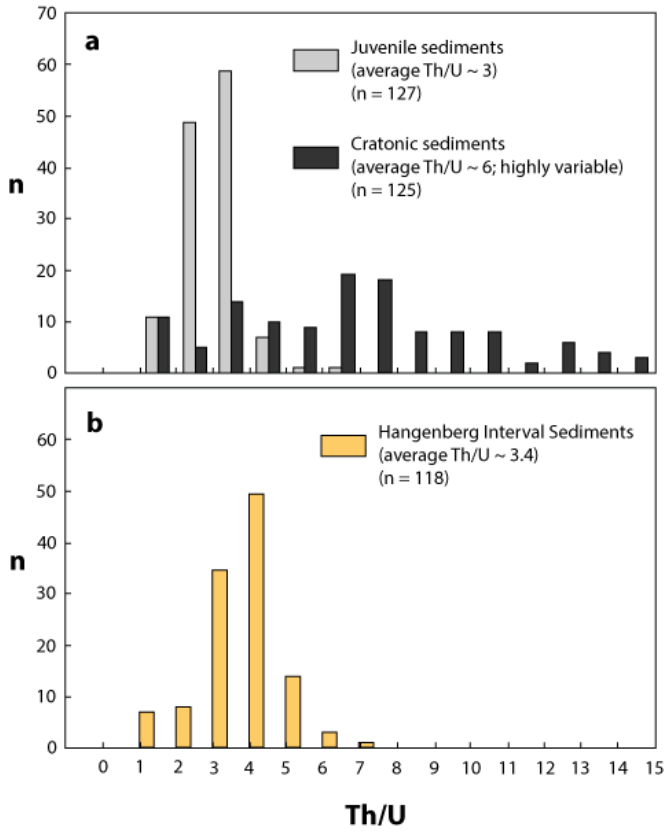


Fig. 6. (a) Th/U ratios in modern sediments can be used to show sedimentary provenance, where Th/U ratios clustered ~3 indicate a juvenile sediment source (light gray bars); in comparison, more mature cratonic sediments (black bars) have higher average Th/U ratios (~6) and more variability (modified after Carpentier et al. (2013)). (b) Th/U ratios in the Heishantou Formation boundary cluster ~3.4, indicating a juvenile sediment source, consistent with an island arc.

jointing, or hydrothermal alteration within the zone of the isotope excursion at the tentative D–C boundary in the Heishantou Formation, and therefore interpret the $^{87}Sr/^{86}Sr$ excursion as primary.

We are likewise reluctant to assign specific conodont ages to the Heishantou Formation sediments based solely on chemostratigraphic similarities to data sets calibrated to conodont biostratigraphy that has recently been determined to be problematic at the GSSP in France ( Kaiser, 2009, Corradini et al., 2011, Kaiser and Corradini, 2011 and Aretz, 2013), but it should be noted that all four existing data sets that span the D–C boundary do show a strong excursion in $^{87}Sr/^{86}Sr$ values within a meter of the D–C boundary itself ( Kürschner et al., 1993 and Brand et al., 2004) or at the tentative D–C boundary (this study). Therefore we conclude that the D–C boundary is located at 212 m above the base of the section, within the Heishantou Formation (Fig. 8).

### *4.4. Sedimentation rates*

Approximately 245 m of sediments have been measured and described at the Boulongour Reservoir, from the top of the Frasnian into the lower Carboniferous (Carmichael et al., 2014 and Suttner et al., 2014). Sedimentation rates were constrained based on observed conodont biostratigraphy (Suttner et al., 2014) and the chemostratigraphically constrained D–C boundary (this study). Rates range from 0.5 cm/ky to 10 cm/ky (Table 3). These calculated sedimentation rates are consistent with rates calculated for other Late Devonian sections (Chen and Tucker, 2003, Elrick and Hinnov, 2007 and De Vleeschouwer et al., 2013) as well as for modern island arc environments (Reid et al., 1996) that together indicate that sedimentation in an island arc environment during this time period can range from 0.5 to 23 cm/ky.

### *4.5. Geochemical proxies for redox, productivity, and sea level changes*

Despite the absence of a visible black shale facies in the Heishantou Formation, it is possible to use multiple whole rock geochemical proxies and magnetic susceptibility data to detect the changes in oceanic redox conditions, the presence of transgression and regression events, and changes in primary productivity. Reliable detection of water column anoxia is unlikely with a single geochemical proxy for most paleoenvironments, therefore a multiple suites of geochemical, textural, and mineralogical proxies are generally required to adequately characterize oxygen levels. All whole rock geochemistry data are provided in Supplemental Information, Table S3.

As many of the commonly used redox signature elements are also lithologically controlled or exhibit inconsistent behavior depending on the depositional environment (Brumsack, 2006, Tribovillard et al., 2006, Piper and Calvert, 2009 and Ver Straeten et al., 2011), care must be taken when analyzing geochemical proxy signatures across sections with variable sedimentology such as the Heishantou Formation so that changes in sediment composition and mineralogy do not mask or overprint the proxy data. To address the issue of lithologic control on the various proxies used in this study, a series of crossplots using $Al_2O_3$ as a sedimentological control to represent detrital input were constructed. These crossplots and a brief explanation of their interpretation are provided in the Supplemental Information. Commonly used redox and productivity proxies such as excess $SiO_2$, Zn, V, Cu, Ba, and Mn can be used in this study only with caution (if at all) as they exhibit moderate to strong lithologic control (Supplemental Information: Discussion of Lithology and Geochemical Proxies, Fig. S1). Proxies such as As, Sb, Tl, Co, Cr, TOC, total S, authigenic U, Ce anomalies, Ni, Ag, Cd, $P_2O_5$, and Mo show little to no lithologic control and are therefore included as reliable proxies (Fig. 9 and Fig. 10).

#### *4.5.1. Redox proxies*

Elevated TOC and total sulfur have long been associated with oceanic anoxia (Berner, 1984 and Calvert and Pedersen, 1992) and their relevance and use as proxies are described in detail in Tribovillard et al. (2006). Although the Heishantou Formation does not exhibit extreme increases in either TOC or total sulfur, there are visible excursions in both of these proxies in the region surrounding the D–C boundary (Fig. 9).

Vanadium and chromium are both precipitated as hydroxides or adsorbed to particulate matter during bacterial denitrification reactions within a sub-oxic water column (Piper and Calvert, 2009), and V/Cr > 5 has historically been used to indicate anoxic bottom water conditions (Hoffman et al., 1998). Despite the lithologic control on V (Supplemental Data: Fig. S1), the V/Cr ratio is independent of lithology. V/Cr ratios increase dramatically at the D–C boundary (Fig. 9) to > 20, indicating suboxic conditions in the water column. This is consistent with elevated V/Cr ratios in the Hangenberg Event in the Kowala Quarry in Poland (Marynowski et al., 2012), the Exshaw Shale in Canada (data from Caplan and Bustin (1998)) and the Appalachian Basin (Beier and Hayes, 1989, Rimmer, 2004 and Perkins et al., 2008).

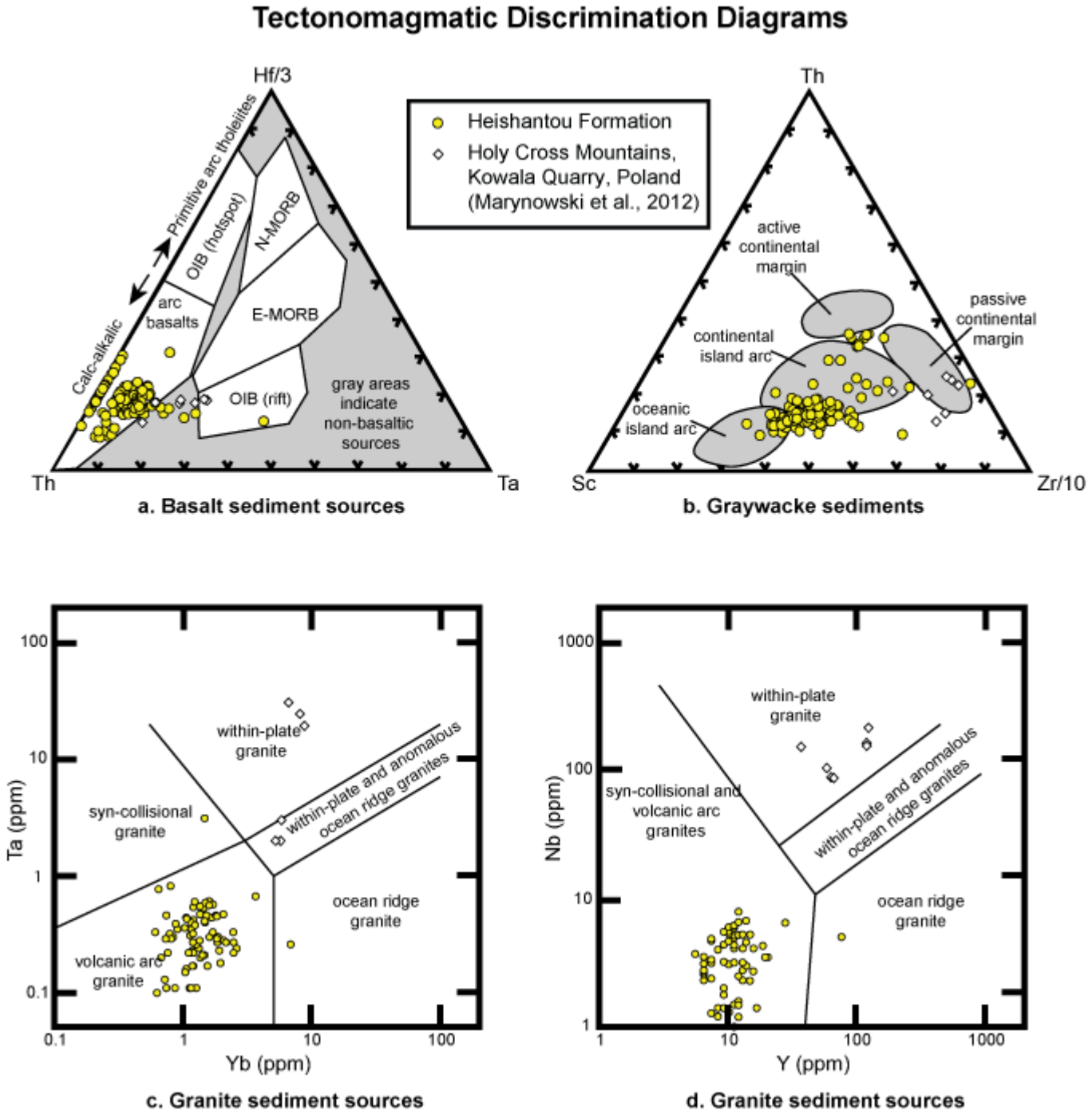


Fig. 7. Sediment source for the Heishantou Formation can be constrained by a number of geochemical signatures. Hf/3–Th–Ta shows sediment source for basalt-derived sediments (Wood, 1980), while Th–Sc–Zr/10 shows source for greywacke sediments (after Bhatia and Crook (1986)). Ta/Tb and Nb/Y ratios (Pearce et al., 1984) provide sources for granite-derived sediments. The Heishantou Formation sediments unequivocally show an island arc signature (either continental or oceanic island arcs) that varies over time, consistent with an accreting series of island arc terranes. Trace element signatures from detrital sediments in the Kowala Quarry in Poland (an extensively characterized D–C boundary section) are shown for comparison (data from Marynowski et al. (2012)).

**Table 1.**
$^{87}Sr/^{86}Sr$ values for the Heishantou Formation (nitric acid leach), normalized to 0.710248 for standard reference NIST-987 (McArthur et al., 2012).

| Sample Name | Stratigraphy (m) | $^{87}Sr/^{86}Sr$ raw | Standard Error | Absolute Error | $^{87}Sr/^{86}Sr$ normalized |
|---|---|---|---|---|---|
| BU001 | 192.58 | 0.707820 | 0.0006 | 0.000008 | 0.707810 |
| BU004-01 | 193.53 | 0.707874 | 0.0008 | 0.000011 | 0.707864 |
| BU004-02 | 196.53 | 0.707404 | 0.0007 | 0.000010 | 0.707394 |
| BU004-03 | 199.48 | 0.707972 | 0.0007 | 0.000010 | 0.707962 |
| BU005 | 204.03 | 0.708166 | 0.0007 | 0.000010 | 0.708156 |
| BU008 | 205.05 | 0.707503 | 0.0006 | 0.000008 | 0.707493 |
| BU015 | 207.30 | 0.708211 | 0.0006 | 0.000008 | 0.708201 |
| BU017 | 208.83 | 0.708211 | 0.0009 | 0.000013 | 0.708201 |
| BU017(base) | 208.93 | 0.707660 | 0.0009 | 0.000013 | 0.707650 |
| BU026 | 211.08 | 0.707434 | 0.0009 | 0.000013 | 0.707424 |
| BU028 | 211.57 | 0.708463 | 0.0006 | 0.000008 | 0.708453 |
| BU029 | 211.63 | 0.708616 | 0.0007 | 0.000010 | 0.708606 |
| BU030a | 211.67 | 0.708531 | 0.0008 | 0.000011 | 0.708521 |
| BU030b | 211.70 | 0.708149 | 0.0007 | 0.000010 | 0.708139 |
| BU030c | 211.79 | 0.709280 | 0.0007 | 0.000010 | 0.709270 |
| BU031 | 211.91 | 0.709270 | 0.0009 | 0.000013 | 0.709260 |
| BU032 | 212.01 | 0.708817 | 0.0007 | 0.000010 | 0.708807 |
| BU033 | 212.16 | 0.709064 | 0.0008 | 0.000011 | 0.709054 |
| BU034 | 212.22 | 0.708486 | 0.0006 | 0.000008 | 0.708476 |
| BU035a | 212.38 | 0.707925 | 0.0007 | 0.000010 | 0.707915 |
| BU035b | 212.53 | 0.708589 | 0.0007 | 0.000010 | 0.708579 |
| BU035c | 212.67 | 0.707912 | 0.0008 | 0.000011 | 0.707902 |
| BU036 | 212.74 | 0.708336 | 0.0006 | 0.000008 | 0.708326 |
| BU037 | 212.76 | 0.707916 | 0.0007 | 0.000010 | 0.707906 |
| BU038 | 212.81 | 0.708109 | 0.0007 | 0.000010 | 0.708099 |
| BU068 | 218.67 | 0.708826 | 0.0009 | 0.000013 | 0.708816 |
| BU070c | 219.44 | 0.707159 | 0.0009 | 0.000013 | 0.707149 |
| BU077 | 220.26 | 0.707242 | 0.0009 | 0.000013 | 0.707232 |
| BU082 | 222.46 | 0.708075 | 0.0009 | 0.000013 | 0.708065 |
| BU089 | 223.78 | 0.708045 | 0.0009 | 0.000013 | 0.708035 |
| BU097 | 230.32 | 0.707739 | 0.0009 | 0.000013 | 0.707729 |
| BU106 | 231.62 | 0.707827 | 0.0006 | 0.000008 | 0.707817 |
| BU112 | 234.59 | 0.707389 | 0.0007 | 0.000010 | 0.707379 |
| BU138 | 245.07 | 0.708188 | 0.0006 | 0.000008 | 0.708178 |
| BU140 | 245.42 | 0.709072 | 0.0006 | 0.000008 | 0.709062 |

Authigenic uranium ($U_{aut}$) sequestration in sediments records a complex redox process, as it is strongly bacterially mediated (Tribovillard et al., 2006) and can be remobilized during diagenesis (Zheng et al., 2002). In specific conditions, however, it can be used as a proxy for anoxia in marine sediments (McManus et al., 2005 and Algeo and Tribovillard, 2009). Authigenic U can be distinguished from detrital U by the Th content of the sediment, which is entirely detrital. It is calculated as $U_{aut} = U_{tot}$ -Th/3, where Th/3 is an estimate of the detrital uranium fraction in typical mudstones (Wignall and Myers, 1988). Fig. 9 shows several prominent $U_{aut}$ excursions in the region immediately surrounding the D–C boundary, although a lack of data on the behavior of $U_{aut}$ in island arc environments limits the reliability of this proxy for detecting anoxia in the Heishantou Formation.

Cerium anomalies in apatite have long been used to show the presence of ocean anoxia (Wilde et al., 1996 and Morad and Felitsyn, 2001) where Ce anomalies with values <− 0.1 are considered to show anoxia. Ce anomalies are calculated using $Ce_{anom} = Log [3Ce_n/(2La_n + Nd_n)]$ (Wright et al., 1987), where "n" indicates REE normalization to the North American Shale Composite (NASC). Ce anomalies show

**Table 2.**
$^{87}Sr/^{86}Sr$ values for the Heishantou Formation (acetic acid leach), normalized to 0.710248 for standard reference NIST-987 (McArthur et al., 2012).

| Sample Name | Stratigraphy (m) | $^{87}Sr/^{86}Sr$ raw | Standard Error | Absolute Error | $^{87}Sr/^{86}Sr$ normalized |
|---|---|---|---|---|---|
| BU004-02 | 196.53 | 0.707388 | 0.0007 | 0.000010 | 0.707378 |
| BU008 | 205.05 | 0.707387 | 0.0009 | 0.000013 | 0.707377 |
| BU015 | 207.30 | 0.707621 | 0.0007 | 0.000010 | 0.707611 |
| BU017 | 208.83 | 0.707680 | 0.0008 | 0.000011 | 0.707670 |
| BU017(base) | 208.93 | 0.707540 | 0.0007 | 0.000010 | 0.707530 |
| BU026 | 211.08 | 0.707203 | 0.0006 | 0.000008 | 0.707193 |
| BU028 | 211.57 | 0.707577 | 0.0007 | 0.000010 | 0.707567 |
| BU029 | 211.63 | 0.707586 | 0.0007 | 0.000010 | 0.707576 |
| BU030a | 211.67 | 0.707653 | 0.0009 | 0.000013 | 0.707643 |
| BU030b | 211.70 | 0.707675 | 0.0007 | 0.000010 | 0.707665 |
| BU030c | 211.79 | 0.707866 | 0.0009 | 0.000013 | 0.707856 |
| BU031 | 211.91 | 0.708162 | 0.0006 | 0.000008 | 0.708152 |
| BU032 | 212.01 | 0.708120 | 0.0007 | 0.000010 | 0.708110 |
| BU034 | 212.22 | 0.708109 | 0.0009 | 0.000013 | 0.708099 |
| BU036 | 212.74 | 0.708115 | 0.0007 | 0.000010 | 0.708105 |
| BU037 | 212.76 | 0.708057 | 0.0007 | 0.000010 | 0.708047 |

scattered anoxia signature within the region of other geochemical anoxia signatures in the Heishantou Formation (Fig. 9).

The concentration of Mo in mudstones is commonly used to show the presence of anoxia in basinal black shales (Tribovillard et al. (2006) and references therein). Because Mo must accumulate under long-term euxinic conditions within restricted basins, elevated concentrations (approximately 50–200 ppm) are not expected to form in unrestricted marine environments (Algeo and Lyons, 2006 and Algeo and Maynard, 2008). There is no enrichment of Mo within the Heishantou Formation at the D–C boundary, but this is not unexpected since we have no sedimentological evidence for the presence of a restricted basin environment, and the tectonic models of the region and sediment source fingerprinting (Fig. 7) do not support the formation of restricted basins at this time. The small spikes in Mo (2–4 ppm) that are apparent throughout the section in the mudstone fraction (Fig. 9) may be due to the presence of turbidites (McKay and Pedersen, 2014).

In addition to those described in detail above, sediment enrichment in arsenic, antimony, cobalt, and thallium can all be used as redox indicators (Brumsack, 2006 and Piper and Calvert, 2009). All of these elements do show enrichment within the region of other geochemical anoxia signatures in the Heishantou Formation (Fig. 9).

### *4.5.2. Sea level and sedimentation proxies*

Geophysical analyses of rock samples produced a distinctive magnetic susceptibility (MS) pattern (Fig. 10), which supports results from microfacies analysis and sedimentological patterns. Although MS signatures can be altered by diagenesis (Riquier et al., 2010), SEM–EDS observations, $^{87}Sr/^{86}Sr$ ratios, and detailed mineralogical analysis of the Heishantou Formation support the idea that the MS signal is driven by detrital components rather than particles of diagenetic origin (see the Supplemental Information for a detailed discussion of the detrital origin of

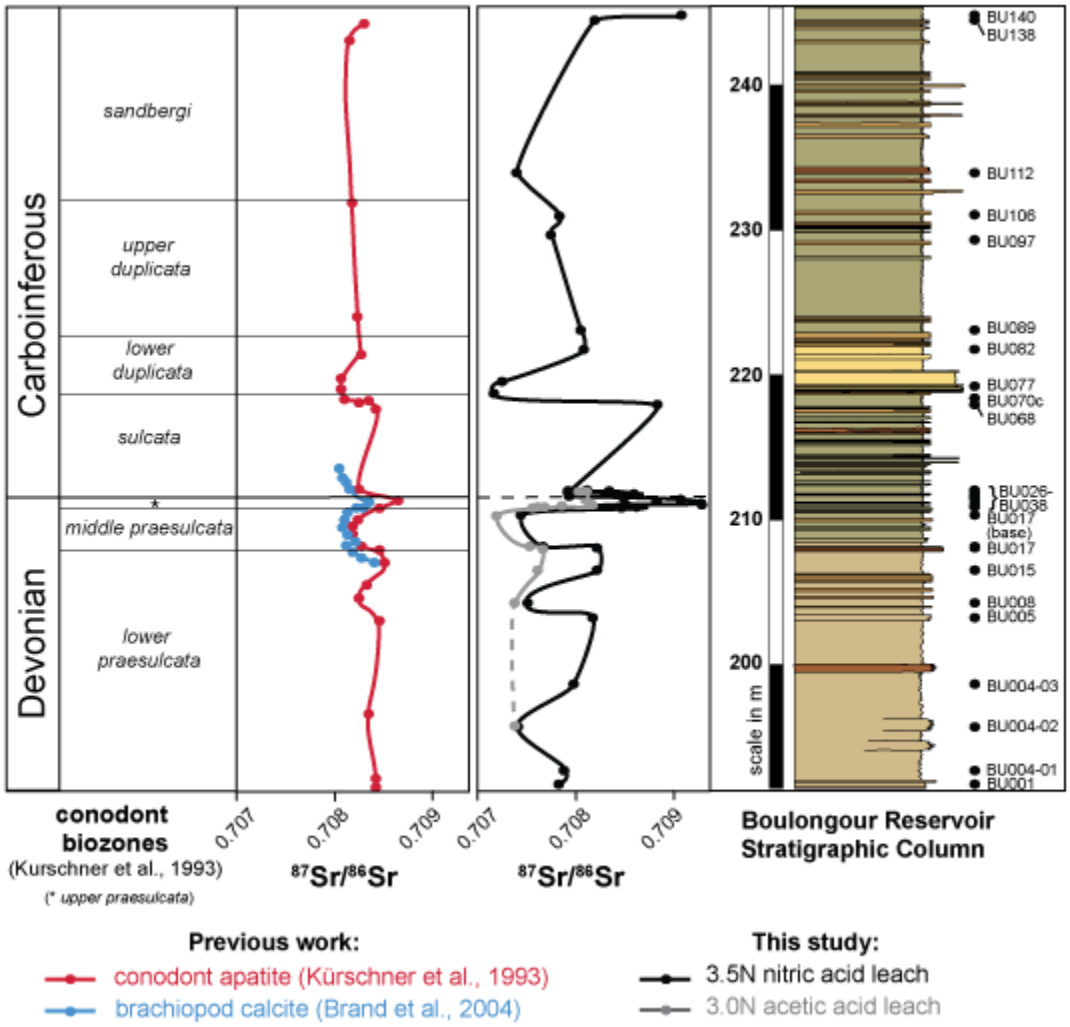


Fig. 8. $^{87}Sr/^{86}Sr$ isotope ratios in bulk sediments (nitric acid leach = black line, acetic acid leach = gray line) show a noticeable excursion at the D–C boundary. Nitric acid leach values line up extremely well with conodont apatite $^{87}Sr/^{86}Sr$ isotope ratios (red line) from Kürschner et al. (1993), and both nitric and acetic leaches mimic the excursion at the D–C boundary in brachiopods (blue line) shown by Brand et al. (2004). Although this study uses bulk sediment rather than single mineral signatures, trends in $^{87}Sr/^{86}Sr$ values clearly denote the D–C boundary, consistent with both previous studies, and can potentially delineate conodont biozones when compared to conodont apatite values. All plotted $^{87}Sr/^{86}Sr$ values (this study and previous studies) are normalized to 0.710248 for standard reference NIST-987 (McArthur et al., 2012). Raw and normalized $^{87}Sr/^{86}Sr$ values from Kürschner et al. (1993) and Brand et al. (2004) are provided in the Supplemental Information (Supplemental Information, Tables S1, S2).

the MS data). A regressive trend marks the base of the unit until sample BU032 (at 212 m), which is followed by a transgressive phase until BU070a (at 264 m). From then on the signal represents a slight, but indistinctive regressive trend until the top of the measured section. A very large excursion reaching up to 1677.4 [10− 9 m3kg− 1] between samples BU052 and BIU055a is related to a volcanic ash layer and does not represent sea level fluctuations. However, all other samples measured are related to sea level fluctuations. Fig. 10 shows an increase in detrital material in the Heishantou Formation just below the D–C boundary, which is consistent with a regression.

### *4.5.3. Productivity proxies*

Phosphorus normalized to the average aluminum content of continental crust is a proxy for authigenic phosphate concentrations, which can be used to show increased biological productivity (Schmitz et al., 1997), necromass deposition (Tribovillard et al., 2006), or hypoxia-induced secondary eutrophication (Middelburg and Levin, 2009).

**Table 3.**
Sedimentation rates of the Boulongour Reservoir section (measured in Suttner et al. (2014)). Sedimentation rates not calculated for sediments above 212 m due to lack of biostratigraphic and chemostratigraphic control.

| Unit | description | thickness (m) | average sedimentation rate | time (Ma) |
|---|---|---|---|---|
| Hongguleleng | intercalated limestones and mudstones | 97 | 2 cm/ky | 5.6 |
| Hebukehe (lower) | intercalated cherts with minor mudstones | 25 | 0.5 cm/ky | 5 |
| Hebukehe (upper) | mudstone | 71 | 5 cm/ky | 0.8 |
| Heishantou (up to 212 m) | intercalated mudstones and bioclastic mudstones | 19 | 10 cm/ky | 2.1 |
| Heishantou (above 212 m) | siltstones with minor sandstone lenses, trace limestone layers | 33 | N/A | N/A |
| *Total* | | *245* | | *13.5* |

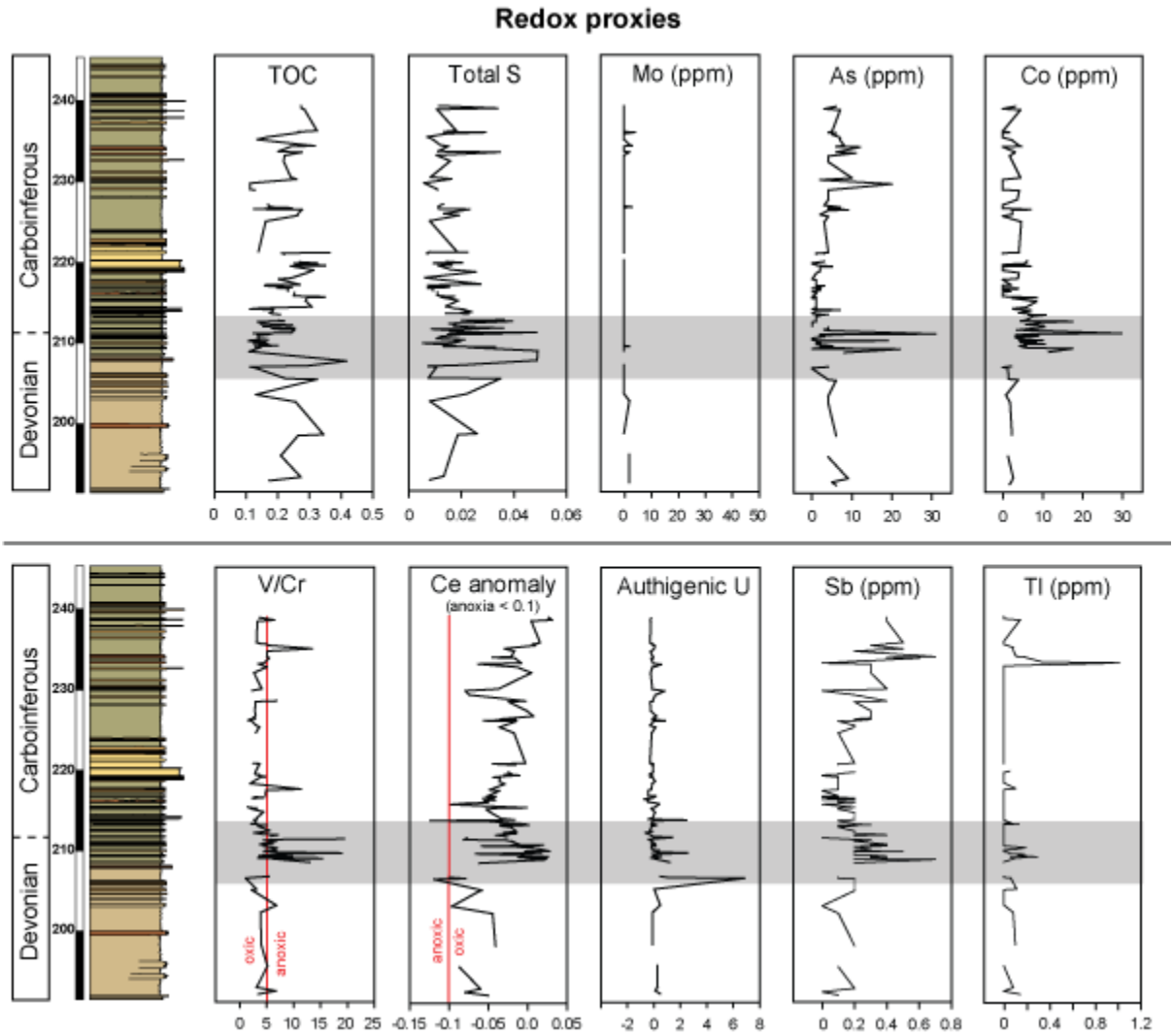


Fig. 9. Whole rock geochemistry of the Heishantou Formation showing commonly used redox proxies: total organic carbon (TOC), total sulfur, Mo, As, Co, V/Cr, Ce anomalies, authigenic U, Sb, and Tl. The proxies used here did not show appreciable lithologic control (color key for sediments in lithologic column provided in Fig. 3). Redox proxies with concentrations that are impacted by lithology are given in the Supplemental Information (Discussion of Lithology and Geochemical Proxies). Shaded areas indicate areas with geochemical signatures consistent with anoxic or suboxic conditions, presumably associated with the Hangenberg Event.

$P2O_5/Al2O_3$ shows a distinct increase at the onset of the regression indicated by MS values (Fig. 10), which is consistent with previous findings in the Hangenberg interval (Beier and Hayes, 1989 and Kumpan et al., 2014b) and has likewise been seen in the Kellwasser Event in the underlying Hongguleleng Formation (Carmichael et al., 2014) as well as in basinal sediments off the Eurasian continental margin (Racki et al., 2002).

Trace element proxies for productivity include silver, which has been found to be a better constrained proxy for productivity than Ba (Tribovillard et al., 2006 and McKay and Pedersen, 2008). Ag shows a distinct yet brief increase in the Heishantou Formation sediments surrounding the D–C boundary (Fig. 10). Nickel is an unusual element that can record either an increased organic carbon flux due to plankton in the photic zone, or bottom water anoxia (Piper and Calvert, 2009). Ni shows an excursion at the D–C boundary location, which is independent of lithology (Fig. 10), but Ni values on their own do not indicate whether they are due to water column anoxia or increased productivity. For V/Ni ratios > 2.5, sedimentary Ni values are due to anoxic bottom water rather than plankton flux (Piper et al., 2007). In the case of the Heishantou Formation nearly all V/Ni ratios > 2.5, but it must be noted that V values are strongly correlated with clay content, leaving the Ni enrichment mechanism (productivity or changes in redox) to remain enigmatic here.

Like nickel, cadmium can be used as a proxy for anoxia (Tribovillard et al., 2006) or productivity (Brumsack, 2006 and Tribovillard et al., 2006). It is coupled with phosphorus during upwelling in suboxic environments (Brumsack, 2006), and can also complex with sulfide species in anoxic/euxinic environments (Tribovillard et al., 2006). Cd shows enrichment in a single sample at the D–C boundary (Fig. 10). As there is no Mo enrichment in the Heishantou Formation sediments (Fig. 9) it is unlikely that euxinic conditions were present, and the excursion in Cd is therefore assigned as a productivity proxy rather than an anoxia proxy.

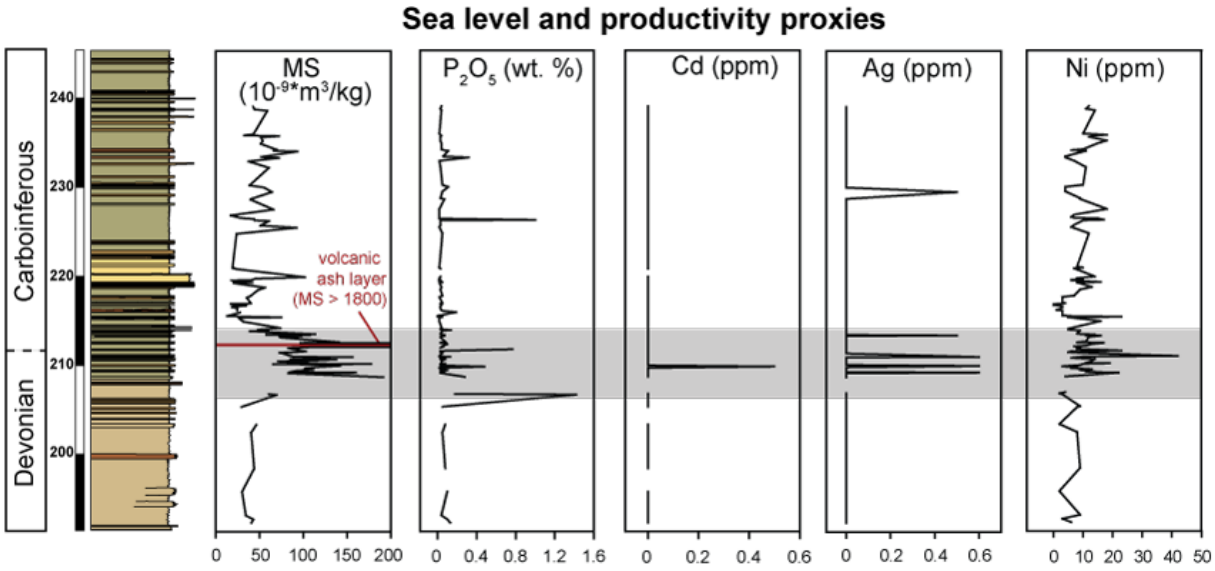


Fig. 10. Whole rock geochemistry of the Heishantou Formation showing proxies for sea level (magnetic susceptibility, MS), and productivity ($P_2O_5$, Cd, Ag, and Ni). The proxies used here did not show appreciable lithologic control (color key for sediments in lithologic column provided in Fig. 3). Productivity proxies with concentrations that are impacted by lithology are described in the Supplemental Information (Lithology and Geochemical Proxies). Shaded areas indicate areas with signatures consistent with anoxic or suboxic conditions, presumably associated with the Hangenberg Event.

#### *4.5.4. Framboidal pyrite*

The size, shape, and distribution of pyrite framboids (circular aggregates of pyrite microcrysts) (Fig. 10), can also be used to assess redox conditions in the water column (Wilkin et al., 1996) and at the sediment–water interface (Wang et al., 2013). Anoxic water columns produce populations of individual or irregularly clumped framboids (generally < 5 μm) with a narrow size range (Wilkin et al., 1996, Wilkin and Barnes, 1997, Wilkin et al., 1997, Wignall and Newton, 1998 and Wang et al., 2013) and may be bacterial in origin (Schieber, 2002, Folk, 2005 and Gong et al., 2008). In fluctuating dysoxic environments, framboids are larger and more variable in size (5–15 μm) (Wignall and Newton, 1998), while samples without framboids are assumed to be deposited under fully oxic conditions or under anoxic conditions without sufficient Fe to form pyrite or its precursor form, greigite (Wilkin and Barnes, 1997). The presence of framboids alone is not sufficient to determine the oxygen levels within the water column, however. Framboids > 25 μm in diameter, or with distinct ovoid morphologies, or that cluster as aggregates with clearly defined edges are likely deposited below the sediment–water interface (Rowan et al., 2009 and Wang et al., 2013) in burrows or pore spaces and do not accurately reflect bottom water oxygenation conditions. Therefore when determining the degree of water column anoxia, care must be taken to analyze not only the size distributions of framboids, but any clustering morphologies and/or framboid shapes.

Iron oxide framboids are present in a variety of intervals throughout the Heishantou Formation, but are particularly abundant in samples from the expected Hangenberg Event interval (Fig. 12). These iron oxide framboids represent oxidation of original pyrite framboids, as some still retain pyrite in the interiors of the framboids crystals. Framboids present in the uppermost part of the Heishantou Formation have morphologies that are consistent with those formed in

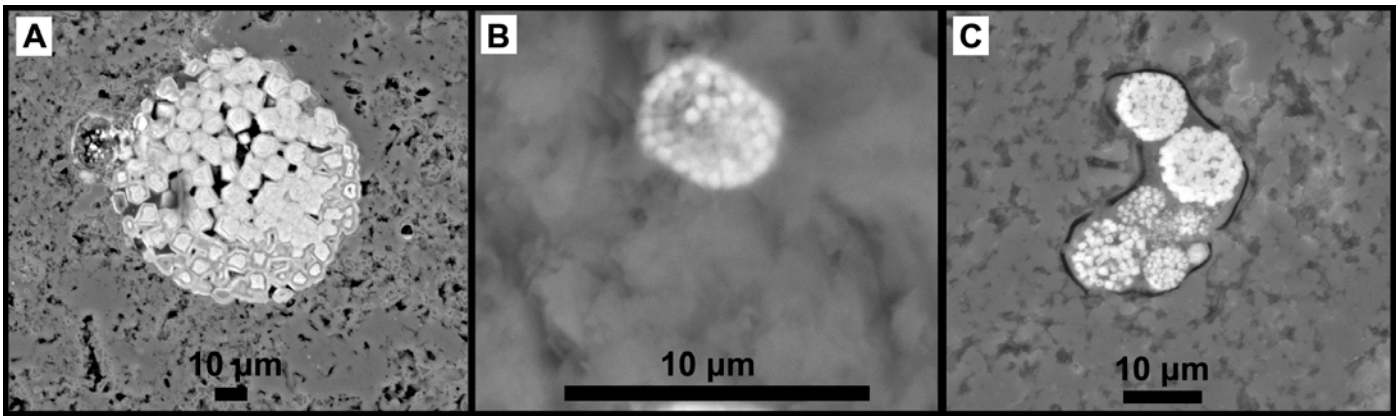


Fig. 11. Backscattered scanning electron microscopy images of framboidal pyrite replaced by magnetite in Heishantou Formation sediments. Framboid size, distribution, and cluster morphologies are variable throughout the Heishantou Formation; framboid formation in sub/dysoxic water column conditions or beneath the sediment–water interface is reflected by a large size range of framboids with average diameters of 10–25 μm (A), while framboids that form within an anoxic water column result in smaller framboids (~5 μm) with a more uniform range of diameters, that are isolated or in irregular clusters, and are generally found in laminated sediments (B). Framboid clusters with clearly defined edges (C) indicate formation in burrows within bioturbated sediments. Framboidal pyrite classifications developed by Wang et al. (2013), Wilkin and Barnes (1997), Wilkin et al. (1996) and Wilkin et al. (1997).

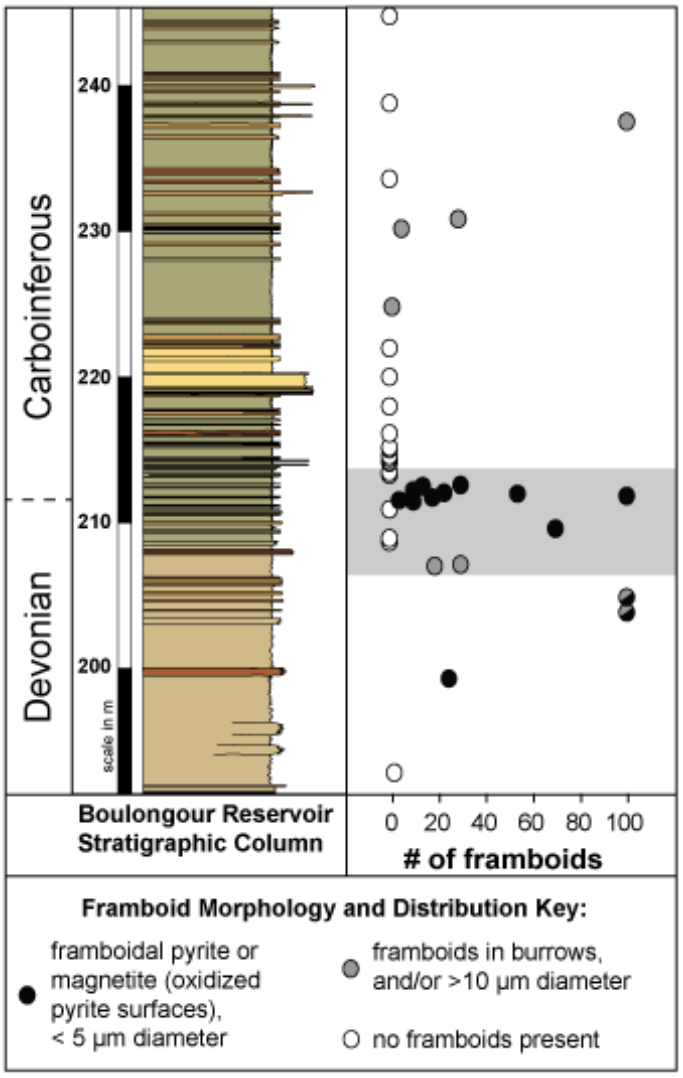


Fig. 12. Framboidal pyrite distribution within Heishantou Formation sediments. Black circles represent isolated or irregular clusters of framboids ~5 mm in diameter, while gray circles represent larger framboids and/or those sequestered in burrows with sharply defined boundaries. White circles indicate that no framboids were present within the sample. The shaded gray region has geochemical proxy signatures consistent with anoxic or suboxic conditions, presumably associated with the Hangenberg Event. Framboidal pyrite distribution supports the location of the Hangenberg Event in the sediments surrounding the D–C boundary. These results are consistent with a series of fluctuating anoxic/dysoxic conditions, but not prolonged euxinic bottom water conditions.

burrowed sediment (Fig. 11C) and do not likely reflect water column anoxia but rather localized anoxia in burrows due to sulfate reducing bacteria below the sediment–water interface.

## 5. Discussion

The lack of reliable conodont biostratigraphy and variable sedimentation makes detection of the D–C boundary and the Hangenberg Event particularly cumbersome in sequences such as the Heishantou Formation that have poor biostratigraphic control and no visible black shale facies. However, we are able to detect not only the D–C boundary but also the Hangenberg Event via whole rock and isotope geochemistry, magnetic susceptibility, framboidal pyrite distribution, and changes in mineral distribution throughout the sediment sequence.

### *5.1. Detection of the D–C boundary*

The similarity of the $^{87}Sr/^{86}Sr$ excursion and oscillations presented in this study with existing $^{87}Sr/^{86}Sr$ studies that have been biostratigraphically constrained, in addition to the general agreement of the calculated sedimentation rates provided by the conodont biostratigraphy with sedimentation rates (both in other sections and calculated independently of $^{87}Sr/^{86}Sr$ data) justifies the use of $^{87}Sr/^{86}Sr$ signatures for chemostratigraphic correlation of the D–C boundary within the Heishantou Formation. Although $^{87}Sr/^{86}Sr$ excursions at the D–C boundary have been shown along continental margins in previous studies (Kürschner et al., 1993 and Brand et al., 2004), detection of these excursions in the Heishantou Formation is significant because these sediments were deposited in a very different tectonic setting than any of the other locations described in previous studies. Regional tectonic studies, local stratigraphy, and sedimentary petrology and geochemistry all indicate that the sequence was deposited on a mid-latitude accreting island arc complex in an open oceanic system, similar to the Marianas Islands (Fig. 2). The presence of this excursion in an open ocean, island arc environment suggests that this excursion could be global in extent and therefore could be used in other locations around the globe to identify the D–C boundary, although additional research across a variety of paleogeographic locations is clearly needed to confirm this.

It is tempting to attribute this excursion to cratonic erosion that occurred with the widespread glaciation that developed in latest Famennian (Isaacson et al., 2008, Brezinski et al., 2010 and McClung et al., 2013), resulting in increased $^{87}Sr$ input to the oceans (Clemens et al., 1993). Late Devonian basinal sediments that have local cratonic sediment sources may exhibit elevated $^{87}Sr/^{86}Sr$ values up to 0.71083 (Lynds et al., 2010), and continental weathering at the D–C boundary was exacerbated not only by changes in sea level but also the erosion of the rising Appalachians by glaciers (Brezinski et al., 2009). It has even been suggested that the tectonic uplift of the Appalachians alone could also have affected seawater $^{87}Sr/^{86}Sr$ ratios (Richter et al., 1992). Invoking glaciation, runoff, and Appalachian tectonics to explain global positive shifts in $^{87}Sr/^{86}Sr$ is problematic, however. Although increased cratonic $^{87}Sr$ may account for some of the increased $^{87}Sr/^{86}Sr$ signatures, the volume of weathered cratonic rock required to produce the magnitude of the positive excursion seen in the open ocean environment of the Heishantou Formation (Fig. 2) would indicate extreme verging on catastrophic cratonic weathering events that are simply not observed in the rock record (Caplan and Bustin, 1999). The reasons for an $^{87}Sr/^{86}Sr$ excursion of this magnitude remain unclear, but the presence of the excursion in three separate locations in very different paleogeographic settings does suggest that the excursion was global in extent.

### *5.2. Detection of the Hangenberg Event*

Although a black shale facies is not visible within the Heishantou Formation, the sea level changes, increased

productivity, and anoxia that characterize the Hangenberg Event can be detected through geochemical proxies such as V/Cr, As, Ag, Ni, Co, magnetic susceptibility and others (Fig. 9 and Fig. 10), and framboidal pyrite distribution (Fig. 11 and Fig. 12). These proxies independently place the Hangenberg Event in the sediments surrounding the D–C boundary, which is where it is expected to be found in places that do contain visible black shale facies.

In the Heishantou Formation, the Hangenberg Event represents a regression/transgression sequence concurrent with a period of fluctuating oxic/dysoxic/anoxic conditions in the water column and variable primary productivity. These fluctuating conditions preserved here are not unexpected due to the isolated, open oceanic paleogeographic location of the site (Fig. 2 and Fig. 7). Although there is a small positive excursion in TOC in the region associated with the Hangenberg Event in the Heishantou Formation despite the lack of a visible black shale unit (Fig. 9), the steep slopes of an island arc would not allow for significant accumulation of organic material as there are no restricted environments in which to store it. Similar fluctuations between dysoxic/anoxic/oxic conditions have likewise been noted in the sediments that record the Kellwasser and Hangenberg Events within euxinic basins or restricted shelf sediments (Beier and Hayes, 1989, Bond et al., 2004, Bond and Wignall, 2005, Schieber, 2009, Kazmierczak et al., 2012, Marynowski et al., 2012 and Kumpan et al., 2014b), open ocean shallow water environments (Carmichael et al., 2014), and platform carbonates (Bond et al., 2013).

A number of the proxies used in this study to detect the Hangenberg Event (Ce anomaly, Tl, Sb, V/Cr, Ag, and occurrence of framboidal pyrite) show additional excursions significantly above the Hangenberg Event (approximately 45–50 m above the base of the section) (Fig. 9, Fig. 10 and Fig. 11). We have no evidence for diagenetic or hydrothermal alteration in these samples, but a lack of biostratigraphic control in this region limits our discussion about the age and significance of these excursions.

### *5.3. Mechanisms for Late Devonian ocean anoxia*

The presence of the Hangenberg Event in an open ocean environment cannot be explained by the causal mechanisms commonly invoked for anoxia events. Many studies in epicontinental settings have concluded that upwelling and subsequent water stratification/stagnation is responsible for anoxia in the Late Devonian (Caplan et al., 1996, McGhee, 1996, Caplan and Bustin, 1999, Riquier et al., 2006, Algeo et al., 2007, Cramer et al., 2008, Chen et al., 2013 and Formolo et al., 2014). Upwelling is an unlikely culprit, however, since paleoclimate modeling shows that it cannot be consistently correlated with organic-rich shales in the Late Devonian (Fig. 13) (Ormiston and Oglesby, 1995). In addition, upwelling in an open ocean environment such as the CAOB would indicate that the entire Late Devonian ocean was overturning (an extraordinary claim that has no evidence to support it). The evidence against widespread, synchronized upwelling during global anoxia events is not new; petroleum geologists have recognized the lack of correlation between upwelling and global oceanic anoxia for more than 30 years (Demaison and Moore, 1980 and references therein).

Although transgression has been invoked as an alternative causal mechanism of anoxia in the Late Devonian (Bond et al., 2004 and Bond and Wignall, 2008), the effects of transgression on a steep slope environment such as an island arc would be negligible in comparison to the effects

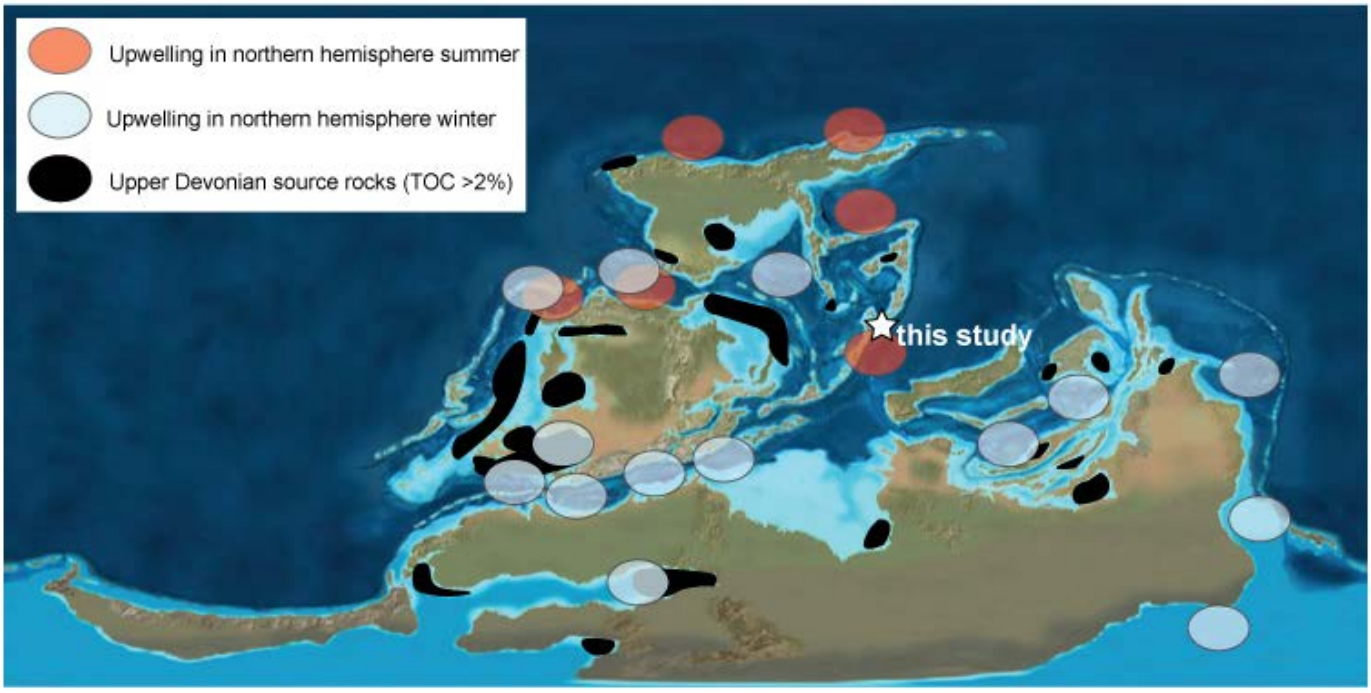


Fig. 13. Climate modeling using reconstructions of the Late Devonian paleogeography shows no correlation between upwelling and organic-rich shale beds. Image adapted from Blakey (2008) and Ormiston and Oglesby (1995).

seen on continental margins or in epicontinental basins. Furthermore, the interplay between sea level and Late Devonian anoxia has recently been called into question (George et al., 2014) as platform carbonates on the continental margins of Australia show no correlation between anoxia and sea level changes.

In contrast, many studies have invoked a "top-down" causal mechanism for Late Devonian ocean anoxia events involving eutrophication due to terrestrially derived nutrients (Caplan and Bustin, 1998, Averbuch et al., 2005, Riquier et al., 2006, Tuite and Macko, 2013, Carmichael et al., 2014, George et al., 2014 and Whalen et al., 2015). This top down eutrophication model (Fig. 14) works along continental margins, epicontinental basins, and in the open ocean along the coastlines of island arcs (Carmichael et al., 2014). It can even work in the open ocean, as Riding (2009) has shown that increased primary productivity at the D–C boundary is coincident with major changes in plankton communities and Paris et al. (1996) show that major blooms of chitinozoans were present at the F–F boundary. It is not yet known if Late Devonian eutrophication was driven only by terrestrial nutrient input and primarily impacted coastlines (as suggested by Whalen et al. (2015)), or if changes in atmospheric $CO_2$ levels caused eutrophication to occur throughout the open ocean.

### *5.4. Triggers for Late Devonian ocean anoxia*

The evolution of land plants has long been invoked as a mechanism for the extreme climate change seen in the Late Devonian (see review by Berner and Kothavala (2001)). Not only did CO2 levels drop precipitously during this time period (Berner and Kothavala, 2001), but geochemical and sedimentary cycles were critically impacted by the onset of soil formation and the stabilizing force of plant roots (Algeo et al., 1995 and Algeo and Scheckler, 1998). Long term climate change related to CO2 drawdown in addition to increased nutrient supply to the oceans has often been invoked as a causal mechanism for Late Devonian ocean anoxia events (see reviews by McGhee (2005); Racki (2005)), but these mechanisms alone do not explain the punctuated, short term timescales of the individual anoxia events. Bolide impacts do explain punctuated, short term events, but there is no evidence for bolide impacts at the D–C boundary (Becker et al., 2012 and Racki, 2012). Tectonic influences such as changing water currents and intensified siliciclastic weathering due to the Variscan/Appalachian orogeny have been invoked to explain the F–F extinction event as well (Copper, 1986 and Averbuch et al., 2005), although correlating the timing of mountain building to short-lived anoxia events remains difficult. More recent work using cyclostratigraphy has found that nearly all of the Late Devonian ocean anoxia events that are paired with major transgressions are associated with climate changes that can be predicted via fluctuations in orbital forcing (De Vleeschouwer et al., 2013 and De Vleeschouwer et al., 2014).

The impact of large igenous provinces on global climate cannot be ignored when postulating the causes of major mass extinctions. The extinction events at the Givetian–Eifelian boundary in the Middle Devonian and the D–C boundary are (so far) some of the only major mass extinctions in the Phanerozoic not directly associated with the emplacement of large igneous provinces (Bond and Wignall, 2014). The correlation of the F–F boundary with the Viluy Traps in Siberia has recently been refined with K/Ar and 40Ar/39Ar age dating (Courtillot et al., 2010 and Ricci et al., 2013). Although a relationship has been suggested between the F–F boundary and the Pripyat–Dniepr–Donets rift system in eastern Russia and the alkaline/carbonatite volcanism on the Kola Peninsula (Kravchinsky, 2012 and Bond and Wignall, 2014), more precise age dates as well as better assessments of magma volume are needed to confirm this link. There is also compelling (albeit conjectural) evidence to suggest that the D–C boundary may also be due to catastrophic igneous activity, but the age dates for the magmatic systems potentially associated with the D–C boundary extinction event are not yet refined enough to make definite connections (Filipiak and Racki, 2010).

Despite more than three decades of research, it is clear that there are still more questions than answers in the quest to understand Late Devonian ocean anoxia events. Taken alone, none of the mechanisms listed above would likely result in global ocean anoxia, although they certainly would put considerable stress on ocean ecosystems. In the absence of unambiguous evidence to suggest that large igneous provinces were the direct cause of the Hangenberg Event, we therefore propose that there is no single trigger mechanism but that a fluctuation in climate at the D–C boundary due to orbital forcing pushed an already vulnerable marine ecosystem into crisis.

## 6. Conclusions and implications

The Late Devonian was a time of prolonged climatic instability caused by a number of factors including rapid change in $CO_2$, changes in the composition and structure of plant ecosystems that led to increased nutrient runoff, the impact of widespread tectonic activity, and perhaps the impact of large igneous provinces. The net result was a series of tipping points that resulted in profound mass extinctions whether measured by taxonomic loss (McGhee et al., 2012) or ecological severity (McGhee et al., 2013). Different taxonomic groups occupying different niches in the ecosystems suffered extinction at different times, suggesting a multifactorial causation that may have depended on interaction of kill mechanisms versus a critical impact from a single factor.

Because our research examines a different geographic area in a fundamentally different tectonic setting (the CAOB) from the majority of previous research on Devonian anoxia, we can begin to constrain some of the factors associated with Late Devonian climate instability and mass extinction. Previous models explaining Late Devonian anoxia required transgression or a similar "bottom up" mechanism to bring deep anoxic water onto an epicontinental shelf. These bottom up models are inconsistent with our findings of anoxia in open oceanic island arc systems in the CAOB. Carmichael et al. (2014) proposed an alternative model for Late Devonian anoxia: shallow water eutrophication caused

by increased nutrient loading (Fig. 14). Our recognition of anoxia associated with the Hangenberg Event also in a shallow water island arc setting in the CAOB provides support for this "top down" eutrophication model. This model is consistent with previous studies that have hypothesized that the ecologically complex, more deeply rooted forests of the Late Devonian could have enhanced weathering and soil formation leading to increased nutrient loading in coastal areas (Algeo et al., 2001, Tuite and Macko, 2013, George et al., 2014 and Whalen et al., 2015), that tectonic uplift caused enhanced nutrient runoff (Averbuch et al., 2005), or that runoff from forest wildfires caused water column eutrophication (Rimmer et al., 2004, Marynowski and Filipiak, 2007 and Marynowski et al., 2012). Our geochemical data from the Kellwasser Event (Carmichael et al., 2014) and the Hangenberg Event (this study) intervals in the CAOB support the model of global increased nutrient loading associated with anoxia in the Late Devonian. The presence of well-developed, lycopsid-dominated plant ecosystems in the terrestrial units directly underlying the Hongguleleng Formation (Xu et al., 2014) indicates that large forests were present even on volcanic island arcs in the CAOB, which further supports the nutrient loading hypothesis as a causal mechanism for anoxia. This is also consistent with the "dead zones" in modern coastal waters, where nutrient loading causes localized anoxia (McGlathery et al., 2007).

Anoxia at the Hangenberg Event is often associated with a major regression and rapid transgression in many epicontinental settings, where relatively small scale fluctuations in sea level can have a major impact on sedimentation. We also see evidence of this regression/transgression couplet in the Heishantou sediments in the CAOB associated with the Hangenberg Event interval via magnetic susceptibility data and changes in sediment distribution, as well as in $^{87}Sr/^{86}Sr$ isotopes (although the mechanism for $^{87}Sr$ enrichment is still unclear). Even though the Heishantou Formation sediments were deposited on an oceanic island arc with a steep slope, they still show evidence for significant sea level changes, which indicates that the sea level changes during the Hangenberg Event were extreme. This further supports the hypothesis that the rapid regression/transgression at the Hangenberg Event was a global eustatic event of significant magnitude.

The unique paleogeography of our studied section allows us to answer questions about the extent and mechanism of the Hangenberg Event and the sea level changes at the D–C boundary that cannot be answered in locations associated with epicontinental margins or basins or the Variscan/Appalachian orogenic events. Additional field and geochemical studies in other Late Devonian island arc accretionary systems (such as northwestern China, southwestern Mongolia, eastern Kazakhstan and in the Altai of Siberia) are needed to further test the hypotheses discussed herein.

## Acknowledgments

Field work in 2005–2012 was supported by the following individuals in addition to the authors: X. Q. Chen, Ruth Mawson, John A. Talent, J. Fryda, D. Mathieson, J. Pickett, Gary D. Webster, and B. Frydova. X. Q. Chen is especially thanked for coordinating field trips and for handling the visa process. Carmichael, Moore, and Batchelor were supported by Appalachian State University. Waters was supported by the Assembling the Echinoderm Tree of Life Project (DEB-1314236), a Temminck Fellowship to the Naturalis Biodiversity Center, Leiden, and Appalachian State University. Kido and Suttner were supported by NAP0001 (subproject of IGCP 497) and NAP0017 (subproject of IGCP 580). MS measurements were realized within research plan RVO 67985831 of the Institute of Geology AS CR, v.v.i. The authors are grateful to Bradley Cramer for the helpful discussions on Sr isotope stratigraphy, and to two anonymous reviewers for their helpful comments. This paper is a contribution to IGCP Project 596 (Climate Change and Biodiversity Patterns in the Mid-Paleozoic) and IGCP Project 580 (Application of Magnetic Susceptibility as a Paleoclimatic Proxy on Paleozoic Sedimentary Rocks).

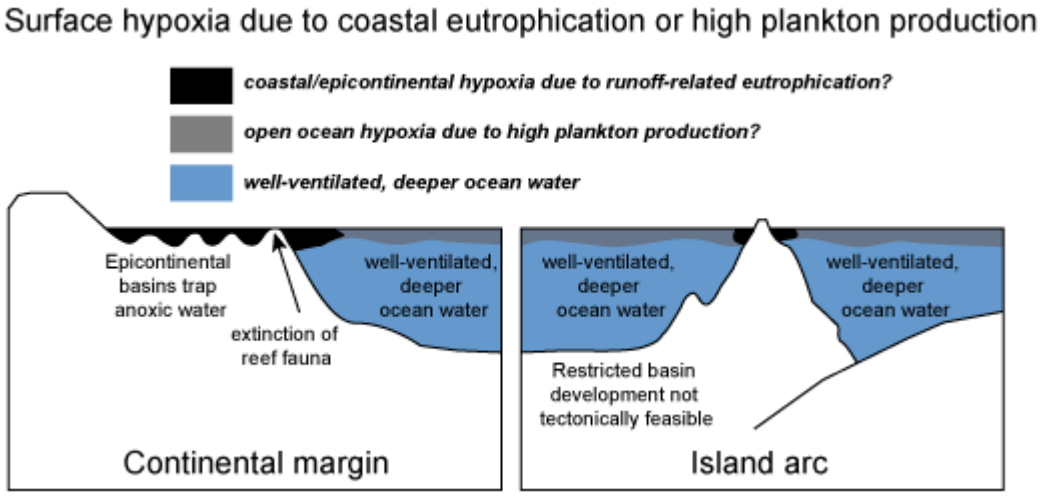


Fig. 14. New model modified from Carmichael et al. (2014) showing an alternative "top down" mechanism for ocean anoxia. On continental margins, shallow waters record episodic dysoxia and anoxia, and black shale facies are common in euxinic basins and/or in shelf sediments with nutrient-rich sediment sources. In island arc environments, shallow waters record episodic dysoxia and anoxia, but organic-rich black shale facies are limited or nonexistent due to topography or nutrient-poor young volcanic sediments. Euxinic basins are not found in island arc environments, as their formation is not tectonically favorable.

**References**


Algeo, T.J., Berner, R.A., Maynard, J.B., Scheckler, S.E., 1995. Late Devonian oceanic anoxic events and biotic crises:"rooted" in the evolution of vascular land plants. GSA today 5, 63-66.

Algeo, T.J., Lyons, T.W., 2006. Mo–total organic carbon covariation in modern anoxic marine environments: Implications for analysis of paleoredox and paleohydrographic conditions. Paleoceanography 21.

Algeo, T.J., Lyons, T.W., Blakey, R.C., Over, D.J., 2007. Hydrographic conditions of the Devono–Carboniferous North American Seaway inferred from sedimentary Mo–TOC relationships. Palaeogeography, Palaeoclimatology, Palaeoecology 256, 204-230.

Algeo, T.J., Maynard, J.B., 2008. Trace-metal covariation as a guide to water-mass conditions in ancient anoxic marine environments. Geosphere 4, 872-887. http://dx.doi.org/10.1130/GES00174.1

Algeo, T.J., Scheckler, S.E., 1998. Terrestrial-marine teleconnections in the Devonian: links between the evolution of land plants, weathering processes, and marine anoxic events. Philosophical Transactions of the Royal Society of London. Series B: Biological Sciences 353, 113-130.

Algeo, T.J., Scheckler, S.E., Maynard, J.B., 2001. Effects of the Middle to Late Devonian spread of vascular land plants on weathering regimes, marine biotas, and global climate. Plants invade the land: Evolutionary and environmental perspectives, 213-236.

Algeo, T.J., Tribovillard, N., 2009. Environmental analysis of paleoceanographic systems based on molybdenum–uranium covariation. Chemical Geology 268, 211-225. http://dx.doi.org/10.1016/j.chemgeo.2009.09.001

Aretz, M., 2013. Report on the workshop of the task group for defining the Devonian-Carboniferous boundary, In: Aretz, M., Richards, B., Kabanov, P., Nikolaeva, S. (Eds.). International Union of Geological Sciences, Subcommission on Carboniferous Stratigraphy, pp. 31-35.

Averbuch, O., Tribovillard, N., Devleeschouwer, X., Riquier, L., Mistiaen, B., Vliet-Lanoe, V., 2005. Mountain building-enhanced continental weathering and organic carbon burial as major causes for climatic cooling at the Frasnian–Famennian boundary (c. 376 Ma)? Terra Nova 17, 25-34.

Azmy, K., Poty, E., Brand, U., 2009. High-resolution isotope stratigraphy of the Devonian–Carboniferous boundary in the Namur–Dinant Basin, Belgium. Sedimentary Geology 216, 117-124. http://dx.doi.org/10.1016/j.sedgeo.2009.03.002

Becker, R., Gradstein, F., Hammer, O., 2012. The Devonian period, In: Gradstein, F.M., Ogg, J.G., Schmitz, M., Ogg, G. (Eds.), The Geologic Time Scale 2012. Elsevier, Amsterdam, pp. 559-601.

Becker, R.T., 1993. Stratigraphische Gliederung und Ammonoideen-Faunen im Nehdenium (Oberdevon II) von Europa und Nord-Afrika. Courier Forschung-Institut Senckenberg 155, 1-405.

Beier, J.A., Hayes, J.M., 1989. Geochemical and isotopic evidence for paleoredox conditions during deposition of the Devonian-Mississippian New Albany Shale, southern Indiana. Geological Society of America Bulletin 101, 774-782. http://dx.doi.org/10.1130/0016-7606(1989)101<0774:gaiefp>2.3.co;2

Berner, R.A., 1984. Sedimentary pyrite formation: An update. Geochimica et Cosmochimica Acta 48, 605-615. http://dx.doi.org/10.1016/0016-7037(84)90089-9

Berner, R.A., Kothavala, Z., 2001. GEOCARB III: A revised model of atmospheric CO2 over Phanerozoic time. American Journal of Science 301, 182-204.

Bhatia, M.R., Crook, K.A.W., 1986. Trace element characteristics of graywackes and tectonic setting discrimination of sedimentary basins. Contr. Mineral. and Petrol. 92, 181-193. http://dx.doi.org/10.1007/BF00375292

Blakey, R., 2008. Late Devonian Paleogeography. Colorado Plateau Geosystems, Inc.

Bond, D., Wignall, P.B., 2005. Evidence for late Devonian (Kellwasser) anoxic events in the Great Basin, western United States. Developments in Palaeontology and Stratigraphy 20, 225-262.

Bond, D., Wignall, P.B., Racki, G., 2004. Extent and duration of marine anoxia during the Frasnian–Famennian (Late Devonian) mass extinction in Poland, Germany, Austria and France. Geological Magazine 141, 173-193.

Bond, D.P., Wignall, P.B., 2008. The role of sea-level change and marine anoxia in the Frasnian–Famennian (Late Devonian) mass extinction. Palaeogeography, Palaeoclimatology, Palaeoecology 263, 107-118.

Bond, D.P., Wignall, P.B., 2014. Large igneous provinces and mass extinctions: An update. Geological Society of America Special Papers 505, SPE505-502.

Bond, D.P., Zatoń, M., Wignall, P.B., Marynowski, L., 2013. Evidence for shallow-water 'Upper Kellwasser'anoxia in the Frasnian–Famennian reefs of Alberta, Canada. Lethaia 46, 355–368. http://dx.doi.org/10.1111/let.12014

Brand, U., 2004. Carbon, oxygen and strontium isotopes in Paleozoic carbonate components: an evaluation of original seawater-chemistry proxies. Chemical Geology 204, 23-44. http://dx.doi.org/10.1016/j.chemgeo.2003.10.013

Brand, U., Legrand-Blain, M., Streel, M., 2004. Biochemostratigraphy of the Devonian−Carboniferous boundary global stratotype section and point, Griotte Formation, La Serre, Montagne Noire, France. Palaeogeography, Palaeoclimatology, Palaeoecology 205, 337-357. http://dx.doi.org/10.1016/j.palaeo.2003.12.015

Brand, U., Tazawa, J.-i., Sano, H., Azmy, K., Lee, X., 2009. Is mid-late Paleozoic ocean-water chemistry coupled with epeiric seawater isotope records? Geology 37, 823-826.

Brezinski, D.K., Cecil, C.B., Skema, V.W., 2010. Late Devonian glacigenic and associated facies from the central Appalachian Basin, eastern United States. Geological Society of America Bulletin 122, 265-281. http://dx.doi.org/10.1130/b26556.1

Brezinski, D.K., Cecil, C.B., Skema, V.W., Kertis, C.A., 2009. Evidence for long-term climate change in Upper Devonian strata of the central Appalachians. Palaeogeography, Palaeoclimatology, Palaeoecology 284, 315-325.

Brumsack, H.-J., 2006. The trace metal content of recent organic carbon-rich sediments: implications for Cretaceous black shale formation. Palaeogeography, Palaeoclimatology, Palaeoecology 232, 344-361.

Buggisch, W., Joachimski, M.M., 2006. Carbon isotope stratigraphy of the Devonian of Central and Southern Europe. Palaeogeography, Palaeoclimatology, Palaeoecology 240, 68-88.

Calvert, S., Pedersen, T., 1992. Organic carbon accumulation and preservation in marine sediments: How important is anoxia. Organic matter: productivity, accumulation, and preservation in recent and ancient sediments 533, 231-263.

Caplan, M.L., Bustin, R.M., 1998. Palaeoceanographic controls on geochemical characteristics of organic-rich Exshaw mudrocks: role of enhanced primary production. Organic Geochemistry 30, 161-188. http://dx.doi.org/10.1016/S0146-6380(98)00202-2

Caplan, M.L., Bustin, R.M., 1999. Devonian–Carboniferous Hangenberg mass extinction event, widespread organic-rich mudrock and anoxia: causes and consequences. Palaeogeography, Palaeoclimatology, Palaeoecology 148, 187-207.

Caplan, M.L., Bustin, R.M., 2001. Palaeoenvironmental and palaeoceanographic controls on black, laminated mudrock deposition: example from Devonian–Carboniferous strata, Alberta, Canada. Sedimentary Geology 145, 45-72. http://dx.doi.org/10.1016/S0037-0738(01)00116-6

Caplan, M.L., Bustin, R.M., Grimm, K.A., 1996. Demise of a Devonian-Carboniferous carbonate ramp by eutrophication. Geology 24, 715-718.

Carmichael, S.K., Waters, J.A., Suttner, T.J., Kido, E., DeReuil, A.A., 2014. A New Model for the Kellwasser Anoxia Events (Late Devonian): Shallow Water Anoxia in an Open Oceanic Setting in the Central Asian Orogenic Belt. Palaeogeography, Palaeoclimatology, Palaeoecology 399, 394-403. http://dx.doi.org/10.1016/j.palaeo.2014.02.016

Carpentier, M., Weis, D., Chauvel, C., 2013. Large U loss during weathering of upper continental crust: The sedimentary record. Chemical Geology 340, 91-104. http://dx.doi.org/10.1016/j.chemgeo.2012.12.016

Chen, D., Qing, H., Li, R., 2005. The Late Devonian Frasnian Famennian (F/F) biotic crisis: Insights from $d^{13}C_{carb}$, $d^{13}C_{org}$ and $^{87}Sr/^{86}Sr$ isotopic systematics. Earth and Planetary Science Letters 235, 151-166.

Chen, D., Tucker, M.E., 2003. The Frasnian–Famennian mass extinction: insights from high-resolution sequence stratigraphy and cyclostratigraphy in South China. Palaeogeography, Palaeoclimatology, Palaeoecology 193, 87-111.

Chen, D., Wang, J., Racki, G., Li, H., Wang, C., Ma, X., Whalen, M.T., 2013. Large sulphur isotopic perturbations and oceanic changes during the Frasnian–Famennian transition of the Late Devonian. Journal of the Geological Society 170, 465-476.

Choulet, F., Faure, M., Cluzel, D., Chen, Y., Lin, W., Wang, B., Jahn, B.-M., 2012. Architecture and evolution of accretionary orogens in the Altaids collage: The early Paleozoic West Junggar (NW China). American Journal of Science 312, 1098-1145.

Clemens, S.C., Farrell, J.W., Gromet, L.P., 1993. Synchronous changes in seawater strontium isotope composition and global climate. Nature 363, 607-610.

Copper, P., 1986. Frasnian/Famennian mass extinction and cold-water oceans. Geology 14, 835-839.

Copper, P., 1994. Ancient reef ecosystem expansion and collapse. Coral Reefs 13, 3-11.

Corradini, C., Kaiser, S.I., Perri, M.C., Spalletta, C., 2011. Protognathodus (Conodonta) and its potential as a tool for defining the Devonian/Carboniferous boundary. Rivista Italiana di Paleontologia e Stratigrafia 117, 15-28.

Courtillot, V., Kravchinsky, V.A., Quidelleur, X., Renne, P.R., Gladkochub, D.P., 2010. Preliminary dating of the Viluy traps (Eastern Siberia): Eruption at the time of Late Devonian extinction events? Earth and Planetary Science Letters 300, 239-245.

Cramer, B., Saltzman, M., Day, J.E., Witzke, B.J., 2008. Record of the Late Devonian Hangenberg global positive carbon-isotope excursion in an epeiric sea setting: carbonate production, organic-carbon burial and paleoceanography during the Late Famennian. Dynamics of Epeiric Seas, Geological Association of Canada Special Paper 48, 103-118.

Da Silva, A., Mabille, C., Boulvain, F., 2009. Influence of sedimentary setting on the use of magnetic susceptibility: examples from the Devonian of Belgium. Sedimentology 56, 1292-1306.

Day, J., Witzke, B., Rowe, H., Ellwood, B., 2013. Magnetic susceptiblity and carbon isotope stratigraphies through the Devonian-Carboniferous boundary interval in the western Illinois basin-central North America, In: Whalen, M., Osadetz, K., Richards, B., Kabanov, P., Weissenberger, J., Potma, K., Koenigshof, P., Suttner, T., Kido, E., Da Silva, A.C. (Eds.), Geophysical and Geochemical Techniques: A window on the Palaeozoic World. IGCP 580 & 596, Calgary, Alberta (Canada), p. 26.

De Vleeschouwer, D., Crucifix, M., Bounceur, N., Claeys, P., 2014. The impact of astronomical forcing on the Late Devonian greenhouse climate. Global and Planetary Change 120, 65-80. http://dx.doi.org/10.1016/j.gloplacha.2014.06.002

De Vleeschouwer, D., Rakociński, M., Racki, G., Bond, D.P., Sobień, K., Claeys, P., 2013. The astronomical rhythm of Late-Devonian climate change (Kowala section, Holy Cross Mountains, Poland). Earth and Planetary Science Letters 365, 25-37.

De Vleeschouwer, D., Whalen, M.T., Day, J.E.J., Claeys, P., 2012. Cyclostratigraphic calibration of the Frasnian (Late Devonian) time scale (western Alberta, Canada). Geological Society of America Bulletin 124, 928-942.

Demaison, G., Moore, G., 1980. Anoxic environments and oil source bed genesis. Organic Geochemistry 2, 9-31.

Du, Y., Gong, Y., Zeng, X., Huang, H., Yang, J., Zhang, Z., Huang, Z., 2008. Devonian Frasnian-Famennian transitional event deposits of Guangxi, South China and their possible tsunami origin. Science in China Series D: Earth Sciences 51, 1570-1580.

Ellwood, B.B., Tomkin, J.H., El Hassani, A., Bultynck, P., Brett, C.E., Schindler, E., Feist, R., Bartholomew, A.J., 2011. A climate-driven model and development of a floating point time scale for the entire Middle Devonian Givetian Stage: A test using magnetostratigraphy susceptibility as a climate proxy. Palaeogeography, Palaeoclimatology, Palaeoecology 304, 85-95.

Elrick, M., Hinnov, L.A., 2007. Millennial-scale paleoclimate cycles recorded in widespread Palaeozoic deeper water rhythmites of North America. Palaeogeography, Palaeoclimatology, Palaeoecology 243, 348-372.

Filipiak, P., Racki, G., 2010. Proliferation of abnormal palynoflora during the end-Devonian biotic crisis. Geological Quarterly 54, 1–14.

Flajs, G., Feist, R., 1988. Index conodonts, trilobites and environment of the Devonian-Carboniferous boundary beds at La Serre (Montagne Noire, France). Courier Forschungsinstitut Senckenberg 100, 53-107.

Folk, R.L., 2005. Nannobacteria and the formation of framboidal pyrite: Textural evidence. Journal of Earth System Science 114, 369-374.

Formolo, M.J., Riedinger, N., Gill, B.C., 2014. Geochemical evidence for euxinia during the Late Devonian extinction events in the Michigan Basin (USA). Palaeogeography, Palaeoclimatology, Palaeoecology 414, 146-154.

Geldsetzer, H.H.J., Goodfellow, W.D., McLaren, D.J., 1993. The Frasnian-Famennian extinction event in a stable cratonic shelf setting: Trout River, Northwest Territories, Canada. Palaeogeography, Palaeoclimatology, Palaeoecology 104, 81-95. http://dx.doi.org/10.1016/0031-0182(93)90121-X

George, A.D., Chow, N., Trinajstic, K.M., 2014. Oxic facies and the Late Devonian mass extinction, Canning Basin, Australia. Geology 42, 327-330. http://dx.doi.org/10.1130/g35249.1

Gharaie, M.H.M., Matsumoto, R., Kakuwa, Y., Milroy, P.G., 2004. Late Devonian facies variety in Iran: volcanism as a possible trigger of the environmental perturbation near the Frasnian-Famennian boundary. Geological Quarterly 48, 323-332.

Gharaie, M.H.M., Matsumoto, R., Racki, G., Kakuwa, Y., 2007. Chemostratigraphy of Frasnian-Famennian transition: Possibility of methane hydrate dissociation leading to mass extinction. Geological Society of America Special Papers 424, 109-125.

Gong, Y.-M., Shi, G.R., Weldon, E.A., Du, Y.-S., Xu, R., 2008. Pyrite framboids interpreted as microbial colonies within the Permian Zoophycos spreiten from southeastern Australia. Geological Magazine 145, 95-103.

Gutak, J.M., Tolokonnikova, Z.A., Ruban, D.A., 2008. Bryozoan diversity in Southern Siberia at the Devonian–Carboniferous transition: New data confirm a resistivity to two mass extinctions. Palaeogeography, Palaeoclimatology, Palaeoecology 264, 93-99. http://dx.doi.org/10.1016/j.palaeo.2008.04.009

Hansen, H., Lojen, S., Toft, P., Dolenec, T., Tong, J., Michaelsen, P., Sarkar, A., 2000. Magnetic susceptibility and organic carbon isotopes of sediments across some marine and terrestrial Permo-Triassic boundaries. Developments in Palaeontology and Stratigraphy 18, 271-289.

Hara, H., Kurihara, T., Kuroda, J., Adachi, Y., Kurita, H., Wakita, K., Hisada, K.-i., Charusiri, P., Charoentitirat, T., Chaodumrong, P., 2010. Geological and geochemical aspects of a Devonian siliceous succession in northern Thailand: Implications for the opening of the Paleo-Tethys. Palaeogeography, Palaeoclimatology, Palaeoecology 297, 452-464. http://dx.doi.org/10.1016/j.palaeo.2010.08.029

Hladil, J., Gersl, M., Strnad, L., Frana, J., Langrova, A., Spisiak, J., 2006. Stratigraphic variation of complex impurities in platform limestones and possible significance of atmospheric dust: a study with emphasis on gamma-ray spectrometry and magnetic susceptibility outcrop logging (Eifelian-Frasnian, Moravia, Czech Republic). International Journal of Earth Sciences 95, 703-723. http://dx.doi.org/10.1007/s00531-005-0052-8

Isaacson, P., Diaz-Martinez, E., Grader, G., Kalvoda, J., Babek, O., Devuyst, F., 2008. Late Devonian–earliest Mississippian glaciation in Gondwanaland and its biogeographic consequences. Palaeogeography, Palaeoclimatology, Palaeoecology 268, 126-142.

Izokh, O., Izokh, N., Ponomarchuk, V., Semenova, D., 2009. Carbon and oxygen isotopes in the Frasnian–Famennian section of the Kuznetsk basin (*southern West Siberia*). Russian Geology and Geophysics 50, 610-617.

Joachimski, M.M., Buggisch, W., 1993. Anoxic events in the late Frasnian—Causes of the Frasnian-Famennian faunal crisis? Geology 21, 675-678.

Joachimski, M.M., Ostertag-Henning, C., Pancost, R.D., Strauss, H., Freeman, K.H., Littke, R., Sinninghe Damsté, J.S., Racki, G., 2001. Water column anoxia, enhanced productivity and concomitant changes in $\delta^{13}C$ and $\delta^{34}S$ across the Frasnian–Famennian boundary (Kowala—Holy Cross Mountains/Poland). Chemical Geology 175, 109-131.

Kaiser, S.I., 2009. The Devonian/Carboniferous boundary stratotype section (La Serre, France) revisited. Newsletters on Stratigraphy 43, 195-205. http://dx.doi.org/10.1127/0078-0421/2009/0043-0195

Kaiser, S.I., Becker, R.T., Steuber, T., Aboussalam, S.Z., 2011. Climate-controlled mass extinctions, facies, and sea-level changes around the Devonian–Carboniferous boundary in the eastern Anti-Atlas (SE Morocco). Palaeogeography, Palaeoclimatology, Palaeoecology 310, 340-364.

Kaiser, S.I., Corradini, C., 2011. The early siphonodellids (Conodonta, Late Devonian-Early Carboniferous): overview and taxonomic state. Neues Jahrbuch für Geologie und Paläontologie-Abhandlungen 261, 19-35.

Kaiser, S.I., Steuber, T., Becker, R.T., 2008. Environmental change during the Late Famennian and Early Tournaisian (Late Devonian–Early Carboniferous): implications from stable isotopes and conodont biofacies in southern Europe. Geological Journal 43, 241-260.

Kaiser, S.I., Steuber, T., Becker, R.T., Joachimski, M.M., 2006. Geochemical evidence for major environmental change at the Devonian–Carboniferous boundary in the Carnic Alps and the Rhenish Massif. Palaeogeography, Palaeoclimatology, Palaeoecology 240, 146-160. http://dx.doi.org/10.1016/j.palaeo.2006.03.048

Kazmierczak, J., Kremer, B., Racki, G., 2012. Late Devonian marine anoxia challenged by benthic cyanobacterial mats. Geobiology 10, 371-383.

Kido, E., Suttner, T.J., Waters, J.A., Ariunchimeg, Y., Gonchigdorj, S., Atwood, J.W., Webster, G.D., 2013. Devonian deposits of the Baruunhuurai Terrane, western Mongolia (IGCP 596 Field Workshop). Episodes 36, 242-254.

Kim, Y., Lee, K.-S., Koh, D.-C., Lee, D.-H., Lee, S.-G., Park, W.-B., Koh, G.-W., Woo, N.-C., 2003. Hydrogeochemical and isotopic evidence of groundwater salinization in a coastal aquifer: a case study in Jeju volcanic island, Korea. Journal of Hydrology 270, 282-294. http://dx.doi.org/10.1016/S0022-1694(02)00307-4

Komatsu, T., Kato, S., Hirata, K., Takashima, R., Ogata, Y., Oba, M., Naruse, H., Ta, P.H., Nguyen, P.D., Dang, H.T., Doan, T.N., Nguyen, H.H., Sakata, S., Kaiho, K., Königshof, P., 2014. Devonian–Carboniferous transition containing a Hangenberg Black Shale equivalent in the Pho Han Formation on Cat Ba Island, northeastern

Vietnam. Palaeogeography, Palaeoclimatology, Palaeoecology 404, 30-43.
Königshof, P., Savage, N.M., Lutat, P., Sardsud, A., Dopieralska, J., Belka, Z., Racki, G., 2012. Late Devonian sedimentary record of the Paleotethys Ocean – The Mae Sariang section, northwestern Thailand. Journal of Asian Earth Sciences 52, 146-157. http://dx.doi.org/10.1016/j.jseaes.2012.03.006
Kravchinsky, V.A., 2012. Paleozoic large igneous provinces of Northern Eurasia: Correlation with mass extinction events. Global and Planetary Change 86, 31-36.
Kumpan, T., Bábek, O., Kalvoda, J., Frýda, J., Matys Grygar, T., 2014a. A high-resolution, multiproxy stratigraphic analysis of the Devonian–Carboniferous boundary sections in the Moravian Karst (Czech Republic) and a correlation with the Carnic Alps (Austria). Geological Magazine 151, 201-215.
Kumpan, T., Bábek, O., Kalvoda, J., Matys Grygar, T., Frýda, J., 2014b. Sea-Level and Environmental Changes Around the Devonian–Carboniferous Boundary in the Namur–Dinant Basin (S Belgium, NE France): A Multi-proxy Stratigraphic Analysis of Carbonate Ramp Archives and its Use in Regional and Interregional Correlations. Sedimentary Geology, DOI:10.1016/j.sedgeo.2014.1006.1007. http://dx.doi.org/10.1016/j.sedgeo.2014.06.007
Kürschner, W., Becker, R.T., Buhl, D., Veizer, J., 1993. Strontium isotopes in conodonts: Devonian-Carboniferous transition, the northern Rhenish Slate Mountains, Germany. Annales de la Société géologique de Belgique 115, 595-622.
Lynds, R., Campbell-Stone, E., Becker, T.P., Frost, C.D., 2010. Stratigraphic evaluation of reservoir and seal in a natural CO2 field : Lower Paleozoic, Moxa Arch, southwest Wyoming. Rocky Mountain Geology 45, 113-132. http://dx.doi.org/10.2113/gsrocky.45.2.113
Ma, X.P., Zong, P., Sun, Y.L., 2011. The Devonian (Famennian) sequence in the western Junggar area, Northern Xinjiang, China. SDS Newsletter 26, 44-49.
Marynowski, L., Filipiak, P., 2007. Water column euxinia and wildfire evidence during deposition of the Upper Famennian Hangenberg event horizon from the Holy Cross Mountains (central Poland). Geological Magazine 144, 569-595.
Marynowski, L., Zatoń, M., Rakociński, M., Filipiak, P., Kurkiewicz, S., Pearce, T.J., 2012. Deciphering the upper Famennian Hangenberg Black Shale depositional environments based on multi-proxy record. Palaeogeography, Palaeoclimatology, Palaeoecology 346, 66-86. http://dx.doi.org/10.1016/j.palaeo.2012.05.020
Matyja, H., Sobie, K., Marynowski, L., 2015. The expression of the Hangenberg Event (latest Devonian) in a relatively shallow-marine succession (Pomeranian Basin, Poland): the results of a multi-proxy investigation. Geological Magazine, 1-29. http://dx.doi.org/10.1017/S001675681400034X
McArthur, J., Howarth, R., Bailey, T., 2001. Strontium isotope stratigraphy: LOWESS version 3: best fit to the marine Sr-isotope curve for 0–509 Ma and accompanying look-up table for deriving numerical age. The Journal of Geology 109, 155-170.
McArthur, J., Howarth, R., Shields, G., 2012. Strontium Isotope Stratigraphy. The Geologic Time Scale 1, 127-144.
McClung, W.S., Eriksson, K.A., Terry Jr, D.O., Cuffey, C.A., 2013. Sequence stratigraphic hierarchy of the Upper Devonian Foreknobs Formation, central Appalachian Basin, USA: Evidence for transitional greenhouse to icehouse conditions. Palaeogeography, Palaeoclimatology, Palaeoecology 387, 104-125. http://dx.doi.org/10.1016/j.palaeo.2013.07.020
McGhee, G.R., 1996. The late Devonian mass extinction: the Frasnian/Famennian crisis. Columbia University Press. p.
McGhee, G.R., 2005. Modelling Late Devonian extinction hypotheses, In: Over, D.J., Morrow, J.R., Wignall, P.B. (Eds.), Developments in Palaeontology and Stratigraphy. Elsevier, pp. 37-50.
McGhee, G.R., 2013. When the Invasion of Land Failed: The Legacy of the Devonian Extinctions. Columbia University Press. 317 p.
McGhee, G.R., Clapham, M.E., Sheehan, P.M., Bottjer, D.J., Droser, M.L., 2013. A new ecological-severity ranking of major Phanerozoic biodiversity crises. Palaeogeography, Palaeoclimatology, Palaeoecology 370, 260-270. http://dx.doi.org/10.1016/j.palaeo.2012.12.019
McGhee, G.R., Sheehan, P.M., Bottjer, D.J., Droser, M.L., 2012. Ecological ranking of Phanerozoic biodiversity crises: The Serpukhovian (early Carboniferous) crisis had a greater ecological impact than the end-Ordovician. Geology 40, 147-150. http://dx.doi.org/10.1130/g32679.1
McGlathery, K.J., Sundback, K., Anderson, I.C., 2007. Eutrophication in shallow coastal bays and lagoons: the role of plants in the coastal filter. Marine Ecology Progress Series 348, 1-18.
McKay, J., Pedersen, T., 2008. The accumulation of silver in marine sediments: A link to biogenic Ba and marine productivity. Global Biogeochemical Cycles 22.
McKay, J.L., Pedersen, T.F., 2014. Geochemical Response to Pulsed Sedimentation: Implications for the Use of Mo as a Paleo-proxy. Chemical Geology 382, 83-94. http://dx.doi.org/10.1016/j.chemgeo.2014.05.009
McManus, J., Berelson, W.M., Klinkhammer, G.P., Hammond, D.E., Holm, C., 2005. Authigenic uranium: Relationship to oxygen penetration depth and organic carbon rain. Geochimica et Cosmochimica Acta 69, 95-108. http://dx.doi.org/10.1016/j.gca.2004.06.023
Middelburg, J., Levin, L., 2009. Coastal hypoxia and sediment biogeochemistry. Biogeosciences Discussions 6, 3655-3706.
Morad, S., Felitsyn, S., 2001. Identification of primary Ce-anomaly signatures in fossil biogenic apatite: implication for the Cambrian oceanic anoxia and phosphogenesis. Sedimentary Geology 143, 259-264.
Murphy, A.E., Sageman, B.B., Hollander, D.J., 2000. Eutrophication by decoupling of the marine biogeochemical cycles of C, N, and P: A mechanism for the Late Devonian mass extinction. Geology 28, 427-430.
Myrow, P.M., Hanson, A., Phelps, A.S., Creveling, J.R., Strauss, J.V., Fike, D.A., Ripperdan, R.L., 2013. Latest Devonian (Famennian) global events in western Laurentia: Variations in the carbon isotopic record linked to diagenetic alteration below regionally extensive unconformities. Palaeogeography, Palaeoclimatology, Palaeoecology 386, 194-209.
Myrow, P.M., Ramezani, J., Hanson, A.E., Bowring, S.A., Racki, G., Rakociński, M., 2014. High-precision U–Pb age and duration of the latest Devonian (Famennian) Hangenberg event, and its implications. Terra Nova 26, 222-229. http://dx.doi.org/10.1111/ter.12090
Myrow, P.M., Strauss, J.V., Creveling, J.R., Sicard, K.R., Ripperdan, R., Sandberg, C.A., Hartenfels, S., 2011. A carbon isotopic and sedimentological record of the latest Devonian (Famennian) from the Western U.S. and Germany. Palaeogeography, Palaeoclimatology, Palaeoecology 306, 147-159. http://dx.doi.org/10.1016/j.palaeo.2011.04.013
Ormiston, A.R., Oglesby, R.J., 1995. Effect of Late Devonian paleoclimate on source rock quality and location, In: Huc, A.Y. (Ed.), Paleogeography, Paleoclimate, and Source Rocks. American Association of Petroleum Geologists, pp. 105-132.
Paris, F., Girard, C., Feist, R., Winchester-Seeto, T., 1996. Chitinozoan bio-event in the Frasnian-Famennian boundary beds at La Serre (Montagne Noire, southern France). Palaeogeography, Palaeoclimatology, Palaeoecology 121, 131-145.
Pearce, J.A., Harris, N.B., Tindle, A.G., 1984. Trace element discrimination diagrams for the tectonic interpretation of granitic rocks. Journal of petrology 25, 956-983.
Perkins, R.B., Piper, D.Z., Mason, C.E., 2008. Trace-element budgets in the Ohio/Sunbury shales of Kentucky: Constraints on ocean circulation and primary productivity in the Devonian–Mississippian Appalachian Basin. Palaeogeography, Palaeoclimatology, Palaeoecology 265, 14-29. http://dx.doi.org/10.1016/j.palaeo.2008.04.012
Piper, D.Z., Calvert, S.E., 2009. A marine biogeochemical perspective on black shale deposition. Earth-Science Reviews 95, 63-96. http://dx.doi.org/10.1016/j.earscirev.2009.03.001
Piper, D.Z., Perkins, R.B., Rowe, H.D., 2007. Rare-earth elements in the Permian Phosphoria Formation: Paleo proxies of ocean geochemistry. Deep Sea Research Part II: Topical Studies in Oceanography 54, 1396-1413. http://dx.doi.org/10.1016/j.dsr2.2007.04.012
Pujol, F., Berner, Z., Stüben, D., 2006. Palaeoenvironmental changes at the Frasnian/Famennian boundary in key European sections: Chemostratigraphic constraints. Palaeogeography, Palaeoclimatology, Palaeoecology 240, 120-145.
Racki, G., 2005. Toward understanding Late Devonian global events: few answers, many questions, In: Over, D.J., Morrow, J.R., Wignall, P.B. (Eds.), Understanding Late Devonian and Permian-Triassic Biotic and Climatic Events: Towards an Integrated Approach, pp. 5-36.
Racki, G., 2012. The Alvarez impact theory of mass extinction; limits to its applicability and the "Great Expectations Syndrome". Acta Palaeontologica Polonica 57, 681-702.
Racki, G., Racka, M., Matyja, H., Devleeschouwer, X., 2002. The Frasnian/Famennian boundary interval in the South Polish–Moravian shelf basins: integrated event-stratigraphical approach. Palaeogeography, Palaeoclimatology, Palaeoecology 181, 251-297.
Reid, P.R., Carey, S.N., Ross, D.R., 1996. Late Quaternary sedimentation in the Lesser Antilles island arc. Geological Society of America Bulletin 108, 78-100. http://dx.doi.org/10.1130/0016-7606(1996)108<0078:LQSITL>2.3.CO;2
Ricci, J., Quidelleur, X., Pavlov, V., Orlov, S., Shatsillo, A., Courtillot, V., 2013. New $^{40}Ar/^{39}Ar$ and K–Ar ages of the Viluy traps (Eastern Siberia):

Further evidence for a relationship with the Frasnian–Famennian mass extinction. Palaeogeography, Palaeoclimatology, Palaeoecology 386, 531-540.
Richter, F.M., Rowley, D.B., DePaolo, D.J., 1992. Sr isotope evolution of seawater: the role of tectonics. Earth and Planetary Science Letters 109, 11-23. http://dx.doi.org/10.1016/0012-821X(92)90070-C
Riding, R., 2009. An atmospheric stimulus for cyanobacterial-bioinduced calcification ca. 350 million years ago? Palaios 24, 685-696.
Rimmer, S.M., 2004. Geochemical paleoredox indicators in Devonian–Mississippian black shales, Central Appalachian Basin (USA). Chemical Geology 206, 373-391. http://dx.doi.org/10.1016/j.chemgeo.2003.12.029
Rimmer, S.M., Thompson, J.A., Goodnight, S.A., Robl, T.L., 2004. Multiple controls on the preservation of organic matter in Devonian–Mississippian marine black shales: geochemical and petrographic evidence. Palaeogeography, Palaeoclimatology, Palaeoecology 215, 125-154. http://dx.doi.org/10.1016/j.palaeo.2004.09.001
Riquier, L., Averbuch, O., Devleeschouwer, X., Tribovillard, N., 2010. Diagenetic versus detrital origin of the magnetic susceptibility variations in some carbonate Frasnian–Famennian boundary sections from Northern Africa and Western Europe: implications for paleoenvironmental reconstructions. International Journal of Earth Sciences 99, 57-73.
Riquier, L., Tribovillard, N., Averbuch, O., Devleeschouwer, X., Riboulleau, A., 2006. The Late Frasnian Kellwasser horizons of the Harz Mountains (Germany): two oxygen-deficient periods resulting from different mechanisms. Chemical Geology 233, 137-155.
Rowan, C.J., Roberts, A.P., Broadbent, T., 2009. Reductive diagenesis, magnetite dissolution, greigite growth and paleomagnetic smoothing in marine sediments: A new view. Earth and Planetary Science Letters 277, 223-235.
Sallan, L.C., Coates, M.I., 2010. End-Devonian extinction and a bottleneck in the early evolution of modern jawed vertebrates. Proceedings of the National Academy of Sciences 107, 10131-10135.
Schieber, J., 2002. Sedimentary pyrite: A window into the microbial past. Geology 30, 531-534.
Schieber, J., 2009. Discovery of agglutinated benthic foraminifera in Devonian black shales and their relevance for the redox state of ancient seas. Palaeogeography, Palaeoclimatology, Palaeoecology 271, 292-300.
Schindler, E., 1993. Event-stratigraphic markers within the Kellwasser Crisis near the Frasnian/Famennian boundary (Upper Devonian) in Germany. Palaeogeography, Palaeoclimatology, Palaeoecology 104, 115-125.
Schmitz, B., Charisi, S.D., Thompson, E.I., Speijer, R.P., 1997. Barium, SiO2 (excess), and P2O5 as proxies of biological productivity in the Middle East during the Palaeocene and the latest Palaeocene benthic extinction event. Terra Nova 9, 95-99.
Smith, M.G., Bustin, R.M., 1998. Production and preservation of organic matter during deposition of the Bakken Formation (Late Devonian and Early Mississippian), Williston Basin. Palaeogeography, Palaeoclimatology, Palaeoecology 142, 185-200. http://dx.doi.org/10.1016/S0031-0182(98)00063-7
Stephens, N.P., Sumner, D.Y., 2003. Late Devonian carbon isotope stratigraphy and sea level fluctuations, Canning Basin, Western Australia. Palaeogeography, Palaeoclimatology, Palaeoecology 191, 203-219.
Stigall, A.L., 2012. Speciation collapse and invasive species dynamics during the Late Devonian "Mass Extinction". GSA Today 22, 4-9.
Suttner, T.J., Kido, E., Chen, X., Mawson, R., Waters, J.A., Frýda, J., Mathieson, D., Molloy, P.D., Pickett, J., Webster, G.D., Frýdová, B., 2014. Stratigraphy and facies development of the marine Late Devonian near the Boulongour Reservoir, northwest Xinjiang, China. Journal of Asian Earth Sciences 80, 101-118. http://dx.doi.org/10.1016/j.jseaes.2013.11.001
Tagarieva, R.C., 2013. Conodont biodiversity of the Frasnian-Famennian boundary interval (Upper Devonian) in the Southern Urals. Bulletin of Geosciences 88, 297-314. http://dx.doi.org/10.3140/bull.geosci.1344
Tribovillard, N., Algeo, T.J., Lyons, T., Riboulleau, A., 2006. Trace metals as paleoredox and paleoproductivity proxies: An update. Chemical Geology 232, 12-32. http://dx.doi.org/10.1016/j.chemgeo.2006.02.012
Tuite, M.L., Jr., Macko, S.A., 2013. Basinward nitrogen limitation demonstrates role of terrestrial nitrogen and redox control of delta 15N in a Late Devonian black shale. Geology [Boulder] Pre-Issue Publication. http://dx.doi.org/10.1130/G34549.1
Van Geldern, R., Joachimski, M., Day, J., Jansen, U., Alvarez, F., Yolkin, E., Ma, X.-P., 2006. Carbon, oxygen and strontium isotope records of Devonian brachiopod shell calcite. Palaeogeography, Palaeoclimatology, Palaeoecology 240, 47-67.
Ver Straeten, C.A., Brett, C.E., Sageman, B.B., 2011. Mudrock sequence stratigraphy: A multi-proxy (sedimentological, paleobiological and geochemical) approach, Devonian Appalachian Basin. Palaeogeography, Palaeoclimatology, Palaeoecology 304, 54-73.
Wang, P., Huang, Y., Wang, C., Feng, Z., Huang, Q., 2013. Pyrite morphology in the first member of the Late Cretaceous Qingshankou Formation, Songliao Basin, Northeast China. Palaeogeography, Palaeoclimatology, Palaeoecology 385, 125-136.
Whalen, M.T., Day, J.E.J., 2010. Cross-basin variations in magnetic susceptibility influenced by changing sea level, paleogeography, and paleoclimate: Upper Devonian, Western Canada sedimentary basin. Journal of Sedimentary Research 80, 1109-1127.
Wignall, P., Newton, R., 1998. Pyrite framboid diameter as a measure of oxygen deficiency in ancient mudrocks. American Journal of Science 298, 537-552.
Wignall, P.B., Myers, K.J., 1988. Interpreting benthic oxygen levels in mudrocks: a new approach. Geology 16, 452-455.
Wilde, P., Quinby-Hunt, M.S., Erdtmann, B.-D., 1996. The whole-rock cerium anomaly: a potential indicator of eustatic sea-level changes in shales of the anoxic facies. Sedimentary Geology 101, 43-53.
Wilkin, R., Barnes, H., 1997. Formation processes of framboidal pyrite. Geochimica et Cosmochimica Acta 61, 323-339.
Wilkin, R., Barnes, H., Brantley, S., 1996. The size distribution of framboidal pyrite in modern sediments: An indicator of redox conditions. Geochimica et Cosmochimica Acta 60, 3897-3912.
Wilkin, R.T., Arthur, M.A., Dean, W.E., 1997. History of water-column anoxia in the Black Sea indicated by pyrite framboid size distributions. Earth and Planetary Science Letters 148, 517-525.
Windley, B.F., Alexeiev, D., Xiao, W., Kröner, A., Badarch, G., 2007. Tectonic models for accretion of the Central Asian Orogenic Belt. Journal of the Geological Society 164, 31-47.
Wood, D.A., 1980. The application of a ThHfTa diagram to problems of tectonomagmatic classification and to establishing the nature of crustal contamination of basaltic lavas of the British Tertiary Volcanic Province. Earth and planetary science letters 50, 11-30.
Wright, J., Schrader, H., Holser, W.T., 1987. Paleoredox variations in ancient oceans recorded by rare earth elements in fossil apatite. Geochimica et Cosmochimica Acta 51, 631-644. http://dx.doi.org/10.1016/0016-7037(87)90075-5
Xiao, W., Huang, B., Han, C., Sun, S., Li, J., 2010. A review of the western part of the Altaids: a key to understanding the architecture of accretionary orogens. Gondwana Research 18, 253-273.
Xiao, W., Santosh, M., 2014. The western Central Asian Orogenic Belt: A window to accretionary orogenesis and continental growth. Gondwana Research 25, 1429-1444. http://dx.doi.org/10.1016/j.gr.2014.01.008
Xu, H.-H., Marshall, J.E., Wang, Y., Zhu, H.-C., Berry, C.M., Wellman, C.H., 2014. Devonian spores from an intra-oceanic volcanic arc, West Junggar (Xinjiang, China) and the palaeogeographical significance of the associated fossil plant beds. Review of Palaeobotany and Palynology 206, 10-22.
Yang, G., Li, Y., Santosh, M., Yang, B., Zhang, B., Tong, L., 2013. Geochronology and geochemistry of basalts from the Karamay ophiolitic mélange in West Junggar (NW China): Implications for Devonian–Carboniferous intra-oceanic accretionary tectonics of the southern Altaids. Geological Society of America Bulletin 125, 401-419. http://dx.doi.org/10.1130/b30650.1
Zheng, Y., Anderson, R.F., van Geen, A., Fleisher, M.Q., 2002. Remobilization of authigenic uranium in marine sediments by bioturbation. Geochimica et Cosmochimica Acta 66, 1759-1772. http://dx.doi.org/10.1016/S0016-7037(01)00886-9
Zheng, Y., Hong-Fei, H., Lian-Fang, Y., 1993. Carbon and oxygen isotope event markers near the Frasnian-Famennian boundary, Luoxiu section, South China. Palaeogeography, palaeoclimatology, palaeoecology 104, 97-104.
Zong, P., Becker, R.T., Ma, X., 2014. Upper Devonian (Famennian) and Lower Carboniferous (Tournaisian) ammonoids from western Junggar, Xinjiang, northwestern China—stratigraphy, taxonomy and palaeobiogeography. Palaeobiodiversity and Palaeoenvironments, 1-44. http://dx.doi.org/10.1007/s12549-014-0171-y

**Supplemental Information**

Contents:

**Supplemental Table S1.** $^{87}Sr/^{86}Sr$ values from Kürschner et al. (1993), normalized to 0.710248 for standard reference NIST-987 (McArthur et al., 2012).

| Location | Sample | Age | Material | Sr ratio | 2sigma | Normalized Sr ratio |
|---|---|---|---|---|---|---|
| Oberrodinghausen | OR15/13* | Sandbergi Zone (T) | Polygn. sp. | 0.708463 | 0.000012 | 0.708468 |
| Oberrodinghausen | OR15/13 | Sandbergi Zone (T) | Polygn. sp. | 0.708445 | 0.000010 | 0.708450 |
| Oberrodinghausen | OR14/8 | Sandbergi Zone | Polygn. sp. | 0.708395 | 0.000010 | 0.708400 |
| Oberrodinghausen | OR13/10 | Sandbergi Zone | Polygn. sp. | 0.708370 | 0.000017 | 0.708375 |
| Oberrodinghausen | OR13/10* | Sandbergi Zone | Polygn. sp. | 0.708470 | 0.000014 | 0.708475 |
| Oberrodinghausen | OR12/12* | Sandbergi Zone | Polygn. sp. | 0.708370 | 0.000040 | 0.708375 |
| Oberrodinghausen | OR10/5• | Upper Duplicata Zone | Polygn. sp. | 0.708393 | 0.000023 | 0.708398 |
| Oberrodinghausen | OR7/18• | Lower Duplicata Zone (T) | Polygn. sp. | 0.708464 | 0.000010 | 0.708469 |
| Oberrodinghausen | OR7/18 | Lower Duplicata Zone (T) | Polygn. sp. | 0.708426 | 0.000022 | 0.708431 |
| Oberrodinghausen | ORS/5 | Lower Duplicata Zone | Polygn. sp. | 0.708334 | 0.000018 | 0.708339 |
| Oberrodinghausen | OR4/6 | Lower Duplicata Zone (B) | Polygn. sp. | 0.708340 | 0.000019 | 0.708345 |
| Oberrodinghausen | OR2/12 | upper Sulcata Zone | Polygn. sp. | 0.708353 | 0.000015 | 0.708358 |
| Oberrodinghausen | ORlli | upper Sulcata Zone | Polygn. sp. | 0.708445 | 0.000016 | 0.708450 |
| Oberrodinghausen | OR1/7 | upper Sulcata Zone | Polygn. sp. | 0.708432 | 0.000017 | 0.708437 |
| Oberrodinghausen | B1.1 | Middle Praesulcata Zone | Bisp. sp. | 0.708389 | 0.000011 | 0.708394 |
| Oberrodinghausen | B1.3 | Middle Praesulcata Zone | Bisp. sp. | 0.708387 | 0.000016 | 0.708392 |
| Oberrodinghausen | B2 | Middle Praesulcata Zone | Bisp. sp. | 0.708367 | 0.000015 | 0.708372 |
| Oberrodinghausen | B3 | Middle Praesulcata Zone (B) | Bisp. sp. | 0.708420 | 0.000008 | 0.708425 |
| Oberrodinghausen | B4 | Lower Praesulcata Zone (T) | Bisp. sp. | 0.708473 | 0.000011 | 0.708478 |
| Oberrodinghausen | BS | Lower Praesulcata Zone | Bisp. sp. | 0.708502 | 0.000017 | 0.708507 |
| Oberrodinghausen | B6 | Lower Praesulcata Zone | Bisp. sp. | 0.708423 | 0.000019 | 0.708428 |
| Oberrodinghausen | B9 | Lower Praesulcata Zone | Bisp. sp. | 0.708387 | 0.000037 | 0.708392 |
| Oberrodinghausen | B12 | Lower Praesulcata Zone | Bisp. sp. | 0.708478 | 0.000017 | 0.708483 |
| Oberrodinghausen | B13 | Lower Praesulcata Zone | Bisp. sp. | 0.708430 | 0.000015 | 0.708435 |
| Oberrodinghausen | B15 | Lower Praesulcata Zone | Bisp. sp. | 0.708447 | 0.000013 | 0.708452 |
| Oberrodinghausen | B16 | Lower Praesulcata Zone | Bisp. sp. | 0.708465 | 0.000022 | 0.708470 |
| Oberrodinghausen | B17 | Lower Praesulcata Zone (B) | Bisp. sp. | 0.708443 | 0.000014 | 0.708448 |

| Location | Sample | Age | Material | Sr ratio | 2sigma | Normalized Sr ratio |
|---|---|---|---|---|---|---|
| Oberrodinghausen | B20 | Upper Expansa Zone | Bisp. sp. | 0.708387 | 0.000020 | 0.708392 |
| Oberrodinghausen | B23 | Upper Expansa Zone . | Bisp. sp. | 0.708561 | 0.000012 | 0.708566 |
| Oberrodinghausen | OR6 | Upper Expansa Zone | Bisp. sp. | 0.708409 | 0.000018 | 0.708414 |
| Oberrodinghausen | BaSS | Upper Postera Zone | Polygn. sp. | 0.708465 | 0.000017 | 0.708470 |
| Oberrodinghausen | ORS | Lower Postera Zone | Polygn. sp. | 0.708372 | 0.000014 | 0.708377 |
| Oberrodinghausen | Bal5 | Lower Trachytera Zone | Polygn. sp. | 0.708333 | 0.000013 | 0.708338 |
| Oberrodinghausen | OR3 | Uppermost Marginifera Zone | Polygn. sp. | 0.708282 | 0.000017 | 0.708287 |
| Oberrodinghausen | OR2 | l. Upper Marginifera Zone | Polygn. sp. | 0.708328 | 0.000018 | 0.708333 |
| Oberrodinghausen | OR1 | Lower Marginifera Zone | Polygn. sp. | 0.708435 | 0.000017 | 0.708440 |
| Hasselbachtal | Ha69 | Duplicata Zone | Polygn. sp. | 0.708303 | 0.000014 | 0.708308 |
| Hasselbachtal | Ha78 | lower Sulcata Zone | Polygn. sp. | 0.708447 | 0.000013 | 0.708452 |
| Hasselbachtal | Ha81 | lower Sulcata Zone | Polygn. sp. | 0.708487 | 0.000022 | 0.708492 |
| Hasselbachtal | Ha83 | lower Sulcata Zone | Polygn. sp. | 0.708413 | 0.000015 | 0.708418 |
| Hasselbachtal | Ha84 | lower Sulcata Zone | Protognathodus kuehni | 0.708618 | 0.000016 | 0.708623 |
| Hasselbachtal | HaLE | Middle Praesulcata Zone | Bisp. sp. | 0.708384 | 0.000014 | 0.708389 |
| Hasselbachtal | Ha44B | Lower Praesulcata Zone | Planovatirostrum richteri | 0.708184 | 0.000015 | 0.708189 |
| Hasselbachtal | Ha29 | Lower Praesulcata Zone | Bisp. sp. | 0.708390 | 0.000012 | 0.708395 |
| Hasselbachtal | Ha18C | Lower Praesulcata Zone | Bisp. sp. | 0.708437 | 0.000013 | 0.708442 |
| Hasselbachtal | Hal8B | Lower Praesulcata Zone | Planovatirostrum richteri | 0.708323 | 0.000016 | 0.708328 |
| Ose | OseB | lower Sulcata Zone | Protognathodus kuehni | 0.708494 | 0.000020 | 0.708499 |
| Ose | OseA2 | Upper Praesulcata Zone | Protognathodus kockeli | 0.708537 | 0.000017 | 0.708542 |
| Riescheid | Ri88 | Texanus Zone | Gnathodus sp. | 0.708063 | 0.000014 | 0.708068 |
| Riescheid | Ri77178 | Anchoralis-latus Zone | Gnathodus sp. | 0.708122 | 0.000012 | 0.708127 |
| Riescheid | Ri77/78 | Anchoralis-latus Zone | Gnathodus sp. | 0.708077 | 0.000013 | 0.708082 |

**Supplemental Table S2**. $^{87}Sr/^{86}Sr$ values from Brand et al. (2004), normalized to 0.710248 for standard reference NIST-987 (McArthur et al., 2012). Samples noted with a * represents subsequent uncertainty in sample age assignment, due to recent work demonstrating the lack of reliable index fossils within the GSSP (La Serre section, Montagne Noire, France) (Aretz, 2013; Corradini et al., 2011; Kaiser, 2009; Kaiser and Corradini, 2011)

| Sample | Bed | Conodont zone | Unit | Ca | Mg | Sr | Mn | Fe | $\delta^{18}O$ | $\delta^{13}C$ | $^{87}Sr/^{86}Sr$ (raw) | $^{87}Sr/^{86}Sr$ (normalized) |
|---|---|---|---|---|---|---|---|---|---|---|---|---|
| LSF-5 | 93 | S. sulcata | Griotte | 369120 | 2048 | 1283 | 1025 | 216 | -4.29 | 2.14 | | |
| LSF-8 | 93 | | | 348684 | 2789 | 880 | 3156 | 53 | | | | |
| LSF-9 | 93 | | | | | | | | -4.16 | 2.64 | 0.708203 | 0.708211 |
| LSF-10 | 93 | | | 359710 | 2222 | 1029 | 1025 | 228 | -2.99 | 2.01 | 0.708157 | 0.708165 |
| LSF-27m | 93 | matrix | | 339286 | 3418 | 317 | 4535 | 572 | | | | |
| LSF-22 | 92 | S. sulcata | Griotte | | | | | | -5.74 | 2.32 | | |
| LSF-23m | 92 | matrix | | 357287 | 2915 | 418 | 2341 | 529 | -3.31 | 1.11 | | |
| LSF-6 | 91 | S. sulcata | Griotte | 348791 | 1692 | 1011 | 689 | 176 | | | 0.708169 | 0.708177 |
| LSF-11 | 89 | S. sulcata | Griotte | | | | | | -2.65 | -1.63 | | |
| LSF-12 | 89 | | | | | | | | -2.64 | -3.70 | 0.708229 | 0.708237 |
| LSF-13 | 89 | | | | | | | | -4.05 | 1.55 | | |
| LSF-19 | 89 | | | 352147 | 1999 | 979 | 1582 | 535 | -2.99 | 1.27 | 0.708211 | 0.708219 |
| LSF-20 | 89 | | | | | | | | -2.92 | 2.36 | | |
| LSF-24m | 89 | matrix | | 358048 | 2807 | 356 | 2086 | 711 | | | | |
| GP-03 | | S. sulcata | Glen Park | 407115 | 942 | 1036 | 248 | 288 | -4.11 | 1.31 | 0.708115 | 0.708123 |
| GP-04 | | | | 340328 | 967 | 679 | 363 | 395 | | | | |
| GP-05 | | | | 412600 | 980 | 1244 | 239 | 267 | -3.28 | 1.76 | 0.708113 | 0.708121 |
| *ML-1129 | 87–85 | Upper S. praesulcata | Griotte | | | | | | | | 0.708253 | 0.708261 |
| *ML-1128 | 87–85 | Upper S. praesulcata | Griotte | | | | | | | | 0.708227 | 0.708235 |
| *ML-1128A | 87–85 | | | | | | | | | | 0.708196 | 0.708204 |
| *ML-1128B | 87–85 | matrix | | | | | | | | | 0.708286 | 0.708294 |
| *ML-1128C | 87–85 | | | | | | | | | | 0.708251 | 0.708259 |
| LSF-1A | 82u | Middle S. praesulcata | Griotte | 366901 | 936 | 994 | 137 | 22 | -0.11 | 5.02 | 0.708163 | 0.708171 |
| LSF-1B | 82u | | | 359761 | 1235 | 916 | 301 | 142 | -0.49 | 4.47 | | |
| LSF-2 | 82u | | | 365899 | 93 | 1071 | 197 | 20 | -0.75 | 4.90 | | |

| Sample | Bed | Conodont zone | Unit | Ca | Mg | Sr | Mn | Fe | $\delta^{18}O$ | $\delta^{13}C$ | $^{87}Sr/^{86}Sr$ (raw) | $^{87}Sr/^{86}Sr$ (normalized) |
|---|---|---|---|---|---|---|---|---|---|---|---|---|
| LSF-15A | 82u | | | 365542 | 1022 | 1306 | 105 | 57 | -0.27 | 4.66 | | |
| LSF-16 | 82u | Middle S. praesulcata | Griotte | 368801 | 864 | 1300 | 77 | 68 | | | 0.708152 | 0.708160 |
| LSF-17 | 82u | | | 374556 | 986 | 1104 | 194 | 110 | -0.18 | 4.63 | | |
| LSF-3 | 82l | Middle S. praesulcata | Griotte | 370459 | 1169 | 962 | 438 | 285 | -2.34 | 4.42 | | |
| LSF-4 | 82l | | | 354149 | 3527 | 996 | 213 | 145 | -2.65 | 4.71 | 0.708199 | 0.708207 |
| LSF-14 | 81 | Middle S. praesulcata | Griotte | 347548 | 2045 | 787 | 1142 | 178 | -2.18 | 2.86 | | |
| LSF-18 | 81 | | | 371937 | 662 | 1063 | 127 | 115 | | | 0.708148 | 0.708156 |
| LSF-21 | 81 | | | 388900 | 601 | 1148 | 35 | 51 | | | 0.708145 | 0.708153 |
| LSF-28m | 81 | matrix | | 316267 | 2754 | 280 | 1364 | 672 | -2.94 | 1.59 | | |
| LSF-7 | 79 | Middle S. praesulcata | Griotte | 359333 | 1289 | 1177 | 300 | 204 | -3.14 | 3.16 | 0.708152 | 0.708160 |
| LSF-26m | 79 | matrix | | 307377 | 2684 | 301 | 970 | 968 | | | | |
| *ULL-03 | top of unit | Middle S. praesulcata | Louisiana | 405967 | 545 | 1305 | 51 | 89 | -1.03 | 6.80 | 0.708140 | 0.708148 |
| *ULL-04 | top | | | | | | | | -1.22 | 5.88 | | |
| *ULL-05 | top | | | 377909 | 1921 | 890 | 134 | 431 | -2.73 | 4.87 | | |
| *ULL-05w | top | | | 409681 | 2580 | 996 | 113 | 298 | -2.37 | 5.24 | 0.708156 | 0.708164 |
| *ULL-6m | top | matrix | | | 1715 | 166 | 385 | 637 | -3.97 | 1.68 | 0.708458 | 0.708466 |
| *MLL-01 | below | Middle S. praesulcata | Louisiana | 383058 | 1418 | 1131 | 29 | 40 | -1.42 | 6.04 | 0.708137 | 0.708145 |
| *MLL-02 | below | | | 347994 | 1061 | 1228 | 13 | 10 | -0.68 | 6.67 | 0.708133 | 0.708141 |
| *MLL-02d | below | | | 381531 | 1037 | 1162 | 13 | 5 | -0.59 | 6.72 | | |
| *MLL-7m | below | matrix | | | 2207 | 381 | 130 | 488 | -4.15 | 4.88 | 0.708285 | 0.708293 |
| *LL-01 | Middle | S. praesulcata | Louisiana | 423302 | 557 | 2002 | 51 | 52 | -0.71 | 4.45 | 0.708122 | 0.708130 |
| *LL-02 | | | | 411522 | 630 | 2198 | 63 | 48 | -1.75 | 4.35 | 0.708122 | 0.708130 |
| *LL-03 | | | | 395874 | 1056 | 1847 | 63 | 67 | -0.81 | 4.33 | | |
| *LL-04 | | | | 432037 | 954 | 1461 | 188 | 370 | -0.95 | 4.11 | 0.708131 | 0.708139 |
| *LL-05 | | | | 432203 | 534 | 1610 | 51 | 38 | | | | |
| St-07 | Lower | S. praesulcata | Wocklum | 332990 | 1250 | 1350 | 50 | 110 | -6.57 | 1.32 | 0.708242 | 0.708250 |
| St-08 | | | | 380620 | 1130 | 1350 | 105 | 175 | -7.35 | 1.05 | | |
| St-08b | | | | | | | | | -7.25 | 1.13 | | |

**Supplemental Table S3**. Whole rock geochemistry, magnetic susceptibility (MS), Total Organic Carbon (TOC), and total sulfur data for the Heishantou Formation (available via electronic file).

**Supplemental Information: Lithology and Geochemical Proxies**

The following proxies ($SiO_2$, V, Ti, Zn, Ba, Cu, and Mn) all show some degree of lithologic control when measured against $Al_2O_3$ as a detrital sediment proxy (Figure S1). The relationship between magnetic susceptibility (MS) and lithology is shown in Figure S2. Lithologies were broadly divided into four groups (albite sandstones, bioclastic mudstones, chlorite-illite mudstones, and quartz siltstones) according to whole rock geochemistry and lithologic assignments were confirmed with field observations, X-ray diffraction, and scanning electron microscopy (SEM). Most of the lithologies showed similar trends when plotted against $Al_2O_3$, with the exception of the albite sandstone sandstone group which consistently plots with a different trend. Sediment source analysis using trace elements Th, Zr, and Sc shows that the albite sandstone appears to be derived from an active continental margin rather than an island arc (Figure 7b, main text). The presence of a lens of sandstone derived from a different source would not be unexpected in an accreting terrane, although the systematics of this change in sedimentation remain ambiguous.

*Excess $SiO_2$*

Excess $SiO_2$ can be used as a proxy for primary productivity, representing opaline silica from the detritus of silicic organisms (Schmitz et al., 1997). In the Heishantou Formation, excess $SiO_2$ is obscured by lithological changes (Figure S1).

*Manganese*

Mn is a highly reactive element with multiple valence states, and is used in a variety of biological transformations along redox boundaries. Mn oxidation and reduction reactions have long been recognized as important proxies for anoxia (Frakes and Bolton, 1984; Hulth et al., 1999). However, the use of Mn as an anoxia proxy is highly problematic, as it easily transforms from biogenic oxyhydroxides back to a reduced form, depending on highly localized redox conditions (Tribovillard et al., 2006). Figure S1 primarily shows a correlation between Mn and $Al_2O_3$ in the carbonate fraction, which is not unexpected for rocks that have undergone minor diagenetic reactions, where carbonates incorporate reduced Mn below the sediment-water interface (Brumsack, 2006).

*Barium*

Ba was proposed as a proxy for primary productivity over two decades ago (Dymond et al., 1992), and since then has been frequently used to show signals of increased productivity or decaying biomass related to extinction events (see review by Tribovillard et al., 2006). However, it is difficult to make broad characterizations regarding Ba abundance in the oceans, as local factors such as topography, runoff, Ba-rich plagioclase sediment sources, hydrothermal activity, or remobilization during diagenesis can have as much an impact (or more) on Ba than primary productivity (McManus et al., 1998; Paytan et al., 2007; Paytan et al., 2002; Von Breymann et al., 1992). In the case of the Heishantou Formation, increases in Ba may be due to increases in primary productivity, but it is more likely that the signal simply reflects changes in lithology (Figure S1), as Ba is highly correlated with $Al_2O_3$ content.

*Copper*

Cu is removed from the water column through adsorbtion to Fe-Mn oxyhydroxides or through ligand formation (Algeo and Maynard, 2004). Cu is enriched in sediments only under persistent anoxic or euxinic conditions, while in suboxic or fluctuating oxic/suboxic conditions, it will likely show no enrichment at all (Algeo and Maynard, 2004; Tribovillard et al., 2006). Figure S1 shows that Cu appears to be correlated with the clay-bearing fraction of the sediment. As the clay-bearing fraction is generally representative of the *in situ* decay of Fe and Mg bearing mineral phases rather than direct sedimentation, it is likely that the Cu is correlated with these detrital sediments rather than organic complexes.

*Zinc*

Zn concentrations can be used to assess hydrothermal input (Brumsack, 2006; Tribovillard et al., 2006) as well as oxygenation levels (Algeo and Maynard, 2004; Bond et al., 2004), but its behavior within the water column is not well constrained due to the variety of input sources, the biological uptake and remineralization processes, and the numerous ways it can be complexed with organic acids (Piper and Calvert, 2009; Tribovillard et al., 2006). In the Heishantou Formation, Zn appears to be lithologically controlled (primarily enriched within the clay mineral fraction) (Figure S1).

*Vanadium*

V substitutes for Al in clay minerals during diagenesis (Tribovillard et al., 2006) and there is a distinct but scattered correlation between V and $Al_2O_3$ in the clay mineral fraction of Heishantou Formation sediments (Figure S1). There is no correlation between Cr and detrital sedimentation, however, and when V/Cr ratios are plotted against $Al_2O_3$, the correlation disappears. Therefore V alone was not used as a proxy for anoxia for clay-rich sediments, while V/Cr showed excursions in the sediments surrounding the D-C boundary (Figure 9, main text).

*Magnetic Susceptibility (MS)*

In epicontinental margins or basins, detrital sediments are iron limited and assumed to be uniform in bulk composition. In these scenarios, any change in MS signals can be associated with increased sediment flux associated with sea level change or later diagenetic alteration of original magnetic signatures (Riquier et al., 2010). On active margins such as island arcs, however, sediments are more iron rich (with iron partitioned into a number of different mineralogical phases) and changes in MS signatures can be obscured by varying sediment sources and rates of sedimentation. Therefore, MS signatures from these settings require extensive characterization of the detrital sediment mineralogy in order to parse out the potential role of diagenetic alteration as the cause of MS oscillations.

The method for determination of diagenetic signatures versus sea level signatures is optimized for epicontinental settings (Riquier et al., 2010), but is decidedly more complex in island arc environments. To assess the role of sea level in the MS oscillations in the Heishantou Formation, MS was compared with the detrital proxies $Al_2O_3$, Zr, and Th (Figure S2). With undifferentiated plots, there appears to be no correlation between MS and detrital proxies listed above, but when differentiated by lithology (albite sandstones, bioclastic mudstones, chlorite-illite mudstones, and quartz siltstones), trends are visible. The high correlation between total Fe and MS is present and expected, and there is a noticeable correlation between MgO and MS (showing the impact of chlorite-illite clays on increased MS signatures) (Figure S2). In

epicontinental settings, this correlation is often the result of diagenetic alteration during the smectite-illite transformation of detrital clays (Katz et al., 2000), but in the Heishantou Formation, illite and chlorite are primary detrital clays present (Figure 4 in main text) from the *in situ* weathering of Fe-rich phases such as biotite and hornblende (Figure 5 in main text). The lack of correlation between MS values and framboids altered from pyrite to Fe-oxides and the lack of correlation between MS values and $^{87}Sr/^{86}Sr$ isotope signatures (Figure S2) is further evidence against a diagenetic origin for the MS excursion seen at the D-C boundary in the Heishantou Formation.

**Supplemental Figure S1**. Redox and productivity proxies $SiO_2$, MnO, Ba, Zn, V, and Cu exhibiting moderate to strong lithologic control ($Al_2O_3$ used as a proxy for detrital input).

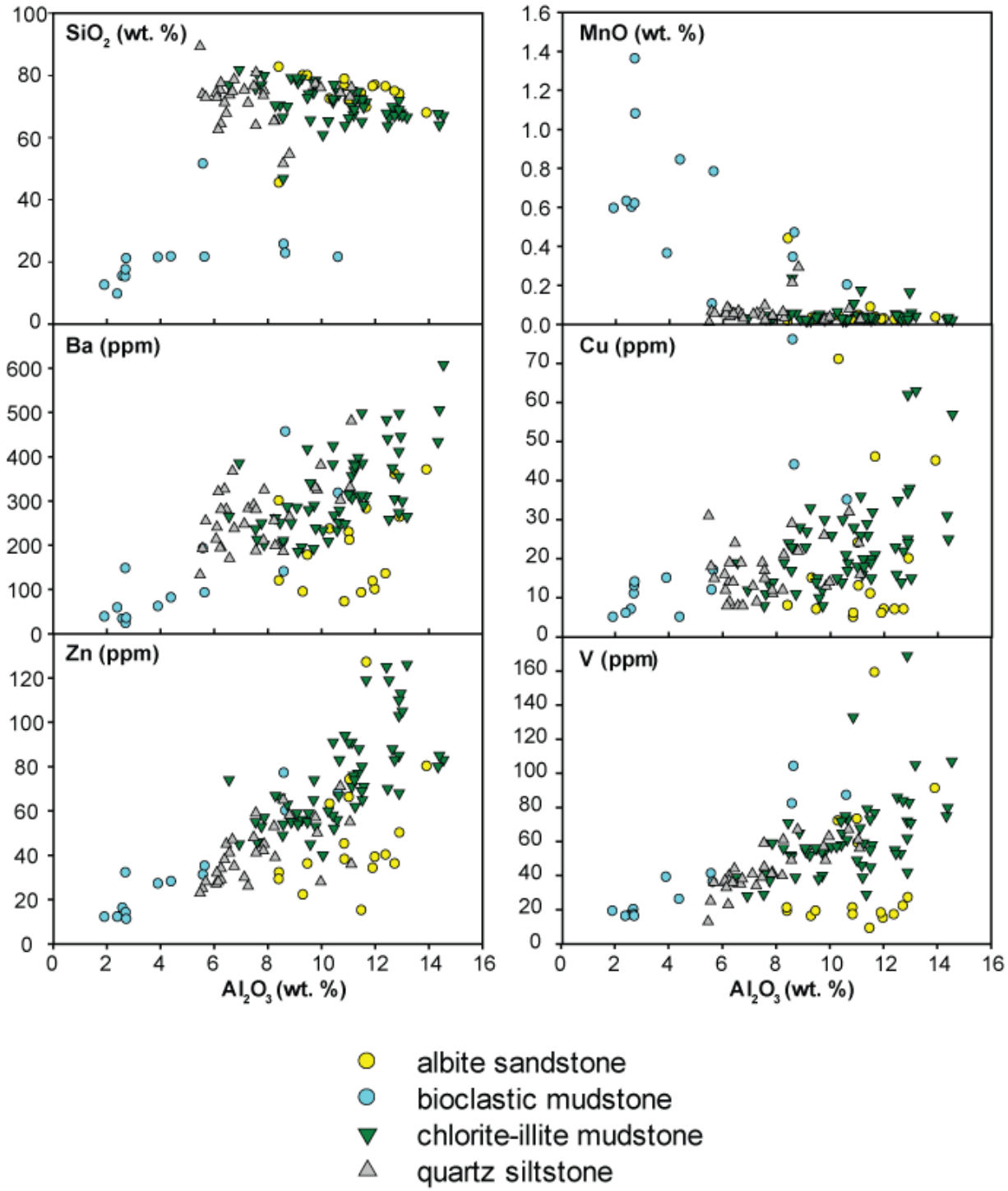

**Supplemental Figure S2**. Correlation plots between MS and detrital proxies $Al_2O_3$, Zr, and Th, as well as total $Fe_2O_3$, MgO (proxy for chlorite-illite clay content), number of Fe oxide framboids (altered pyrite), and $^{87}Sr/^{86}Sr$ ratios. Data points are differentiated by lithology.

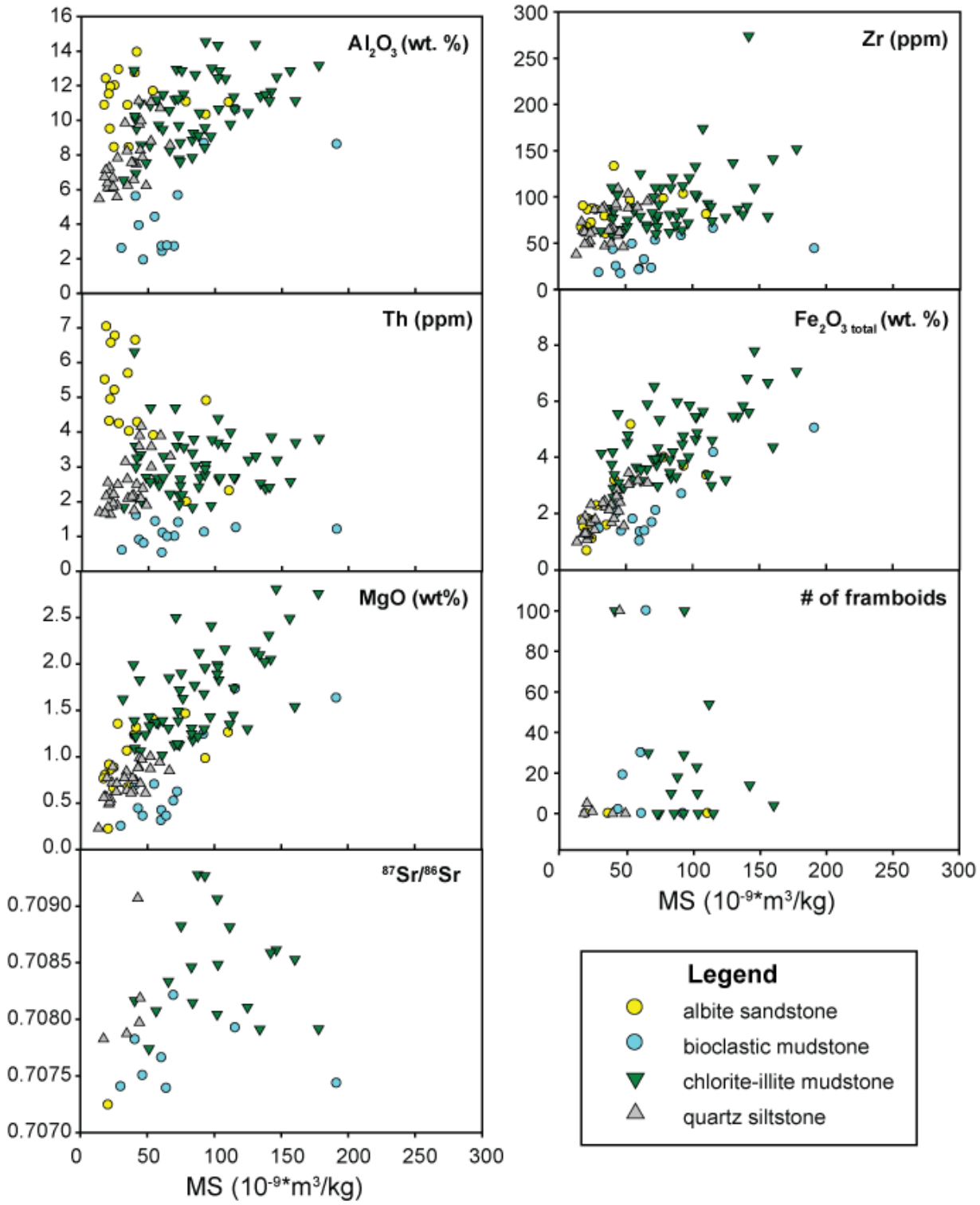

**Supplemental Information: References**


Algeo, T.J., Maynard, J.B., 2004. Trace-element behavior and redox facies in core shales of Upper Pennsylvanian Kansas-type cyclothems. Chemical Geology 206, 289-318. http://dx.doi.org/10.1016/j.chemgeo.2003.12.009

Aretz, M., 2013. Report on the workshop of the task group for defining the Devonian-Carboniferous boundary, In: Aretz, M., Richards, B., Kabanov, P., Nikolaeva, S. (Eds.). International Union of Geological Sciences, Subcommission on Carboniferous Stratigraphy, pp. 31-35.

Bond, D., Wignall, P.B., Racki, G., 2004. Extent and duration of marine anoxia during the Frasnian–Famennian (Late Devonian) mass extinction in Poland, Germany, Austria and France. Geological Magazine 141, 173-193.

Brand, U., Legrand-Blain, M., Streel, M., 2004. Biochemostratigraphy of the Devonian−Carboniferous boundary global stratotype section and point, Griotte Formation, La Serre, Montagne Noire, France. Palaeogeography, Palaeoclimatology, Palaeoecology 205, 337-357. http://dx.doi.org/10.1016/j.palaeo.2003.12.015

Brumsack, H.-J., 2006. The trace metal content of recent organic carbon-rich sediments: implications for Cretaceous black shale formation. Palaeogeography, Palaeoclimatology, Palaeoecology 232, 344-361.

Corradini, C., Kaiser, S.I., Perri, M.C., Spalletta, C., 2011. Protognathodus (Conodonta) and its potential as a tool for defining the Devonian/Carboniferous boundary. Rivista Italiana di Paleontologia e Stratigrafia 117, 15-28.

Dymond, J., Suess, E., Lyle, M., 1992. Barium in deep-sea sediment: A geochemical proxy for paleoproductivity. Paleoceanography 7, 163-181.

Frakes, L., Bolton, B., 1984. Origin of manganese giants: Sea-level change and anoxic-oxic history. Geology 12, 83-86.

Hulth, S., Aller, R.C., Gilbert, F., 1999. Coupled anoxic nitrification/manganese reduction in marine sediments. Geochimica et Cosmochimica Acta 63, 49-66.

Kaiser, S.I., 2009. The Devonian/Carboniferous boundary stratotype section (La Serre, France) revisited. Newsletters on Stratigraphy 43, 195-205. http://dx.doi.org/10.1127/0078-0421/2009/0043-0195

Kaiser, S.I., Corradini, C., 2011. The early siphonodellids (Conodonta, Late Devonian-Early Carboniferous): overview and taxonomic state. Neues Jahrbuch für Geologie und Paläontologie-Abhandlungen 261, 19-35.

Katz, B., Elmore, R.D., Cogoini, M., Engel, M.H., Ferry, S., 2000. Associations between burial diagenesis of smectite, chemical remagnetization, and magnetite authigenesis in the Vocontian trough, SE France. Journal of Geophysical Research: Solid Earth (1978–2012) 105, 851-868.

Kürschner, W., Becker, R.T., Buhl, D., Veizer, J., 1993. Strontium isotopes in conodonts: Devonian-Carboniferous transition, the northern Rhenish Slate Mountains, Germany. Annales de la Société géologique de Belgique 115, 595-622.

McArthur, J., Howarth, R., Shields, G., 2012. Strontium Isotope Stratigraphy. The Geologic Time Scale 1, 127-144.

McManus, J., Berelson, W.M., Klinkhammer, G.P., Johnson, K.S., Coale, K.H., Anderson, R.F., Kumar, N., Burdige, D.J., Hammond, D.E., Brumsack, H.J., 1998. Geochemistry of

barium in marine sediments: Implications for its use as a paleoproxy. Geochimica et Cosmochimica Acta 62, 3453-3473.
Paytan, A., Averyt, K., Faul, K., Gray, E., Thomas, E., 2007. Barite accumulation, ocean productivity, and Sr/Ba in barite across the Paleocene–Eocene Thermal Maximum. Geology 35, 1139-1142.
Paytan, A., Mearon, S., Cobb, K., Kastner, M., 2002. Origin of marine barite deposits: Sr and S isotope characterization. Geology 30, 747-750. http://dx.doi.org/10.1130/0091-7613(2002)030<0747:OOMBDS>2.0.CO;2
Piper, D.Z., Calvert, S.E., 2009. A marine biogeochemical perspective on black shale deposition. Earth-Science Reviews 95, 63-96. http://dx.doi.org/10.1016/j.earscirev.2009.03.001
Riquier, L., Averbuch, O., Devleeschouwer, X., Tribovillard, N., 2010. Diagenetic versus detrital origin of the magnetic susceptibility variations in some carbonate Frasnian–Famennian boundary sections from Northern Africa and Western Europe: implications for paleoenvironmental reconstructions. International Journal of Earth Sciences 99, 57-73.
Schmitz, B., Charisi, S.D., Thompson, E.I., Speijer, R.P., 1997. Barium, SiO2 (excess), and P2O5 as proxies of biological productivity in the Middle East during the Palaeocene and the latest Palaeocene benthic extinction event. Terra Nova 9, 95-99.
Tribovillard, N., Algeo, T.J., Lyons, T., Riboulleau, A., 2006. Trace metals as paleoredox and paleoproductivity proxies: An update. Chemical Geology 232, 12-32. http://dx.doi.org/10.1016/j.chemgeo.2006.02.012
Von Breymann, M.T., Emeis, K.-C., Suess, E., 1992. Water depth and diagenetic constraints on the use of barium as a palaeoproductivity indicator. Geological Society, London, Special Publications 64, 273-284.